

Article

Four-Objective Optimizations for an Improved Irreversible Closed Modified Simple Brayton Cycle

Chenqi Tang^{1,2,3}, Lingen Chen^{1,2,*} , Huijun Feng^{1,2,*} and Yanlin Ge^{1,2}

¹ Institute of Thermal Science and Power Engineering, Wuhan Institute of Technology, Wuhan 430205, China; tangchenqi7@163.com (C.T.); geyali9@hotmail.com (Y.G.)

² School of Mechanical & Electrical Engineering, Wuhan Institute of Technology, Wuhan 430205, China

³ College of Power Engineering, Naval University of Engineering, Wuhan 430033, China

* Correspondence: lgchenna@yahoo.com or lingenchen@hotmail.com (L.C.); huijunfeng@139.com or 1507136871@139.com (H.F.); Tel.: +86-27-836150466 (L.C.); Fax: +86-27-83638709 (L.C.)

Abstract: An improved irreversible closed modified simple Brayton cycle model with one isothermal heating process is established in this paper by using finite time thermodynamics. The heat reservoirs are variable-temperature ones. The irreversible losses in the compressor, turbine, and heat exchangers are considered. Firstly, the cycle performance is optimized by taking four performance indicators, including the dimensionless power output, thermal efficiency, dimensionless power density, and dimensionless ecological function, as the optimization objectives. The impacts of the irreversible losses on the optimization results are analyzed. The results indicate that four objective functions increase as the compressor and turbine efficiencies increase. The influences of the latter efficiency on the cycle performances are more significant than those of the former efficiency. Then, the NSGA-II algorithm is applied for multi-objective optimization, and three different decision methods are used to select the optimal solution from the Pareto frontier. The results show that the dimensionless power density and dimensionless ecological function compromise dimensionless power output and thermal efficiency. The corresponding deviation index of the Shannon Entropy method is equal to the corresponding deviation index of the maximum ecological function.

Keywords: closed simple Brayton cycle; power output; thermal efficiency; power density; ecological function; multi-objective optimization



Citation: Tang, C.; Chen, L.; Feng, H.; Ge, Y. Four-Objective Optimizations for an Improved Irreversible Closed Modified Simple Brayton Cycle. *Entropy* **2021**, *23*, 282. <https://doi.org/10.3390/e23030282>

Academic Editor: Michel Feidt

Received: 17 January 2021

Accepted: 22 February 2021

Published: 26 February 2021

Publisher's Note: MDPI stays neutral with regard to jurisdictional claims in published maps and institutional affiliations.



Copyright: © 2021 by the authors. Licensee MDPI, Basel, Switzerland. This article is an open access article distributed under the terms and conditions of the Creative Commons Attribution (CC BY) license (<https://creativecommons.org/licenses/by/4.0/>).

1. Introduction

Some scholars have studied performances of gas turbine plants (Brayton cycle (BCY)) [1–4] all over the world for their small size and comprehensive energy sources. The gas-steam combined, cogeneration, and other complex cycles have appeared for the requirements of energy conservation and environmental protection. The thermal efficiency (η) of a simple BCY is low, and the NO_x content in combustion product is high. To further improve the cycle performance, it has become a key research direction to improve the initial temperature of the gas or to adopt the advanced cycles (such as regenerative, intercooled, intercooled and regenerative, isothermal heating, and other complex combined cycles).

In the case of simple heating, when the compressible subsonic gas flows through the smooth heating pipe with the fixed cross-sectional area, the gas temperature increases along the pipe direction; in the case of simple region change, when the compressible subsonic gas flows through the smooth adiabatic reductive pipe, the gas temperature decreases along the pipe direction. Based on these two gas properties, the isothermal heating process (IHP) can be realized when the compressible subsonic gas flows through the smooth heating reductive pipe. The combustion chamber, which can recognize the IHP, is called the convergent combustion chamber (CCC). The pipe of the CCC is assumed to be smooth. During the heating process, the temperature of the gas is always constant. According to the energy conservation law, the kinetic energy of the gas increases, that is, the pushing work of

the gas increases. From the definition of enthalpy, it can be seen that enthalpy includes two parts: the thermodynamic energy and the pushing work. Therefore, the enthalpy increases. Based on this, Vecchiarelli et al. [5] proposed the CCC to perform the IHP of the working fluid. The power output (\bar{W}) and η of the BCY could be improved, and the emission of harmful gases such as NO_x could be reduced by adding this combustion chamber model. The regenerative BCYs [6–8] and binary BCY [9] with IHPs were also studied by applying the classical thermodynamics.

Finite time thermodynamics (FTT) is a useful thermodynamic analysis theory and method [10–19]. In general, it is known that Curzon and Ahlborn [12] initialized FTT in 1975. In fact, the classical efficiency bound at the maximum power was also derived by Moutier [10] in 1872 and Novikov [11] in 1957. The applications of FTT include majorly two fields: optimal configurations [20–36] and optimal performances [37–61] studies for thermodynamic cycles and processes. The W and η have been often considered as the optimization objectives (OPOs) of the heat engines [62–72]. When the power density (P) [73–81] was taken as the OPO, the operating unit had a smaller size and higher η . Additionally, the ecological function (E) [82–88] is also an OPO that balances the conflict between W and η .

Kaushik et al. [89] first applied the FTT to studying the regenerative BCY with an IHP. The regenerative, intercooled and regenerative complex BCYs with isothermal heating combustor were further investigated [90–96]. Based on this, Chen et al. [97–99] studied the endoreversible simple isothermal heating BCY with the W , η and E as OPOs. Arora et al. [100,101] adopted NSGA-II and evolutionary algorithms to optimize the irreversible isothermal heating regenerative BCY with the W and η as the OPOs. Chen et al. [102] considered the variable isothermal pressure drop ratio (π_t), established an improved isothermal heating regenerative BCY model, and studied the regenerator's role on cycle performance. Qi et al. [103] demonstrated a closed endoreversible modified binary BCY with IHPs and found the W and η raised as the heat reservoirs' temperature ratios. Tang et al. [104] considered the variable π_t and established an improved irreversible binary BCY model modified by isothermal heating. The heat exchanger's heat conductance distributions (HCDs) and the top and bottom cycles' pressure ratios were taken as optimization variables to optimize the cycle performance.

In the process of the thermodynamic system optimization, single-objective optimization often led to unacceptable objectives for other objectives when there were conflicts among the considered goals. Multi-objective optimization would consider the trade-offs among the goals, and the optimized results were more reasonable [99,100,102,105–125].

In applying the FTT, the heat transfer was introduced into the thermodynamic analysis of the thermodynamic process, and finite temperature difference was considered in Refs. [11,12]. In this paper, the same method in Refs. [11,12] will be used, and the finite temperature difference will be considered when establishing the model, which is the key relation among this paper and the Refs. [11,12]. On this basis, the cycle's irreversibility will be further considered, and the corresponding conclusion will be more in line with the actual situation. The compression and expansion losses in the model in Refs. [97–99] were not considered, and they will be further considered in this paper alongside the losses in the heat exchangers. Meanwhile, the thermal resistance loss and the optimal HCD will be considered. With the W , η , P and E , respectively, as the OPOs, an improved irreversible closed modified simple BCY with one IHP and coupled to variable-temperature heat reservoirs (VTHR) will be optimized, and the optimization results will be compared. The effects of the compressor and turbine efficiencies on optimization results will be analyzed. The NSGA-II algorithm will be applied for multi-objective optimization to obtain the Pareto frontier further. The results obtained in this paper will reveal the original results in Refs. [10–12], which were the initial work of the FTT theory.

2. Cycle Model and Performance Analytical Indicators

The schematic diagram of an improved irreversible closed modified simple BCY with one IHP and coupled to VTHR is shown in Figure 1. A compressor (C), a regular combustion chamber (RCC), a CCC, a turbine (T), and a precooler are the main parts of the cycle. The corresponding $T - s$ diagram of the cycle is shown in Figure 2. The cycle consists of five processes in total:

1. The process $1 \rightarrow 2$ is an irreversible adiabatic compression process in C, and the process $1 \rightarrow 2s$ is an isentropic process corresponding to the process $1 \rightarrow 2$.
2. The process $2 \rightarrow 3$ is an isobaric endothermic process in RCC.
3. The process $3 \rightarrow 4$ is an IHP in CCC. In CCC, the working fluid is isothermally heated, and its flow velocity rises from V_3 to V_4 (the Mach number increases from M_3 to M_4), and its specific enthalpy rises from h_3 to h_4 . The parameter $\pi_t (= p_4/p_3 \leq 1)$ is the isothermal pressure drop ratio. The π_t needs to be given in Refs. [97,98], but the π_t of the improved cycle established in this paper will change with the operation state. The degree of the IHP can be represented by π_t , and the greater the π_t , the greater the degree.
4. The process $4 \rightarrow 5$ is an adiabatic exothermic process in turbine, and the process $4 \rightarrow 5s$ is the isentropic process corresponding to the process $4 \rightarrow 5$.
5. The process $5 \rightarrow 1$ is an isobaric exothermic process in a precooler.

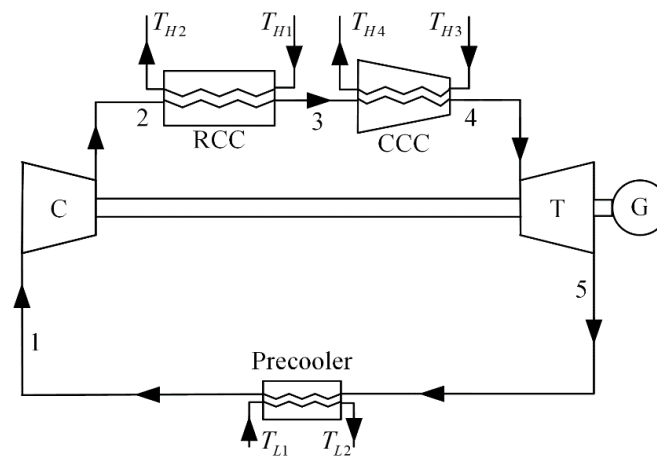


Figure 1. Schematic diagram of the cycle.

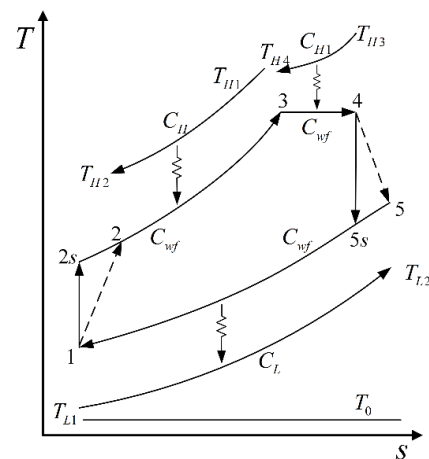


Figure 2. Diagram of the cycle.

The working fluid is the ideal gas. The pressures and temperatures of the working fluid are $p_i (i = 1, 2, 3, 4, 5, 2s, 5s)$ and T_i , and the ratio of specific heat is k . The outside fluids' temperatures are $T_j (j = H1, H2, H3, H4, L1, L2)$. The specific heat at constant pressure and the working fluid's mass flow rate are C_p and \dot{m} . The working fluid's thermal capacity rate is C_{wf} where $C_{wf} = C_p \dot{m}$. The outer fluids' thermal capacity rates at the RCC, CCC, and precooler are C_H, C_{H1} and C_L , respectively; then, one has:

$$C_{Hmax} = \max\{C_H, C_{wf}\}, C_{Lmax} = \max\{C_L, C_{wf}\}, C_{Hmin} = \min\{C_H, C_{wf}\}, C_{Lmin} = \min\{C_L, C_{wf}\} \quad (1)$$

The heat exchangers' heat conductance is the product of the heat transfer coefficient and the heat transfer area. The heat exchangers' heat conductance values in the RCC, CCC, and precooler are U_H, U_{H1} and U_L , the heat transfer units' numbers are N_H, N_{H1} and N_L , and the effectiveness values are E_H, E_{H1} and E_L , respectively:

$$N_H = U_H/C_{Hmin}, N_{H1} = U_{H1}/C_{H1}, N_L = U_L/C_{Lmin} \quad (2)$$

$$E_H = \frac{1 - e^{-N_H(1 - C_{Hmin}/C_{Hmax})}}{1 - (C_{Hmin}/C_{Hmax})e^{-N_H(1 - C_{Hmin}/C_{Hmax})}} \quad (3)$$

$$E_{H1} = 1 - e^{-N_{H1}} \quad (4)$$

$$E_L = \frac{1 - e^{-N_L(1 - C_{Lmin}/C_{Lmax})}}{1 - (C_{Lmin}/C_{Lmax})e^{-N_L(1 - C_{Lmin}/C_{Lmax})}} \quad (5)$$

When $C_{Hmax} = C_{Hmin}$ and $C_{Lmax} = C_{Lmin}$, Equations (3) and (5) are, respectively, simplified as:

$$E_H = N_H/(N_H + 1) \quad (6)$$

$$E_L = N_L/(N_L + 1) \quad (7)$$

The outside fluids' temperature ratios at the RCC and CCC are:

$$\tau_{H1} = T_{H1}/T_0 \quad (8)$$

$$\tau_{H3} = T_{H3}/T_0 \quad (9)$$

where T_0 is the ambient temperature.

The process 1 → 2s is the isentropic one, namely:

$$T_{2s}/T_1 = \pi^m = x \quad (10)$$

where $m = (k - 1)/k$ and π is the pressure ratio of the compressor.

The process 4 → 5s is the isentropic one, namely:

$$T_4/T_{5s} = \pi^m \pi_t^m = xy \quad (11)$$

The process 3 → 4 is the isothermal one, namely:

$$T_3 = T_4 \quad (12)$$

$$\dot{Q}_{3-4} = \dot{m}(h_4 - h_3) - \dot{m} \int_3^4 v dp = -\dot{m} R_g T_3 \ln \pi_t \quad (13)$$

where π_t, M_3 and M_4 must satisfy the following relation:

$$\ln \pi_t = -c_p(k - 1)(M_4^2 - M_3^2)/(2R_g) \quad (14)$$

where the working fluid's flow velocity must be subsonic, namely, $M_3, M_4 < 1$. Because the working fluid has an initial speed, $(M_4^2 - M_3^2) < 0.96$ and $\pi_t > 0.5107$ when $M_3 = 0.2$.

Because of $M_4 > M_3$, $\pi_t < 1$. When $\pi_t = 1$, the cycle model in this paper can be simplified to a simple Brayton cycle.

According to the definition of π_t , it can be obtained that:

$$\pi_t = \frac{p_4}{p_3} = \frac{p_4}{p_3} \cdot \frac{p_1}{p_1} = \frac{p_4}{p_1} \cdot \pi^{-1} \geq \pi^{-1} \quad (15)$$

Considering the irreversibilities in the compressor and the turbine, the efficiencies of them are:

$$\eta_c = (T_1 - T_{2s}) / (T_1 - T_2) \quad (16)$$

$$\eta_t = (T_5 - T_4) / (T_{5s} - T_4) \quad (17)$$

The pressure drop is not considered in this paper. It will be considered in future, as it was by Ref. [126]. The study in Ref. [126] showed that the pressure drop loss has a little influence on the cycle performance quantitatively, and has no influence qualitatively.

The working fluid's heat absorption rates at RCC and CCC are \dot{Q}_{2-3} and \dot{Q}_{3-4} , respectively:

$$\dot{Q}_{2-3} = C_H(T_{H1} - T_{H2}) = C_{wf}(T_3 - T_2) = C_{Hmin}E_H(T_{H1} - T_2) \quad (18)$$

$$\dot{Q}_{3-4} = C_{H1}(T_{H3} - T_{H4}) = C_{H1}E_{H1}(T_{H3} - T_3) = \dot{m}(V_4^2 - V_3^2)/2 \quad (19)$$

The heat releasing rate at the precooler is \dot{Q}_{5-1} , namely:

$$\dot{Q}_{5-1} = C_L(T_{L2} - T_{L1}) = C_{wf}(T_5 - T_1) = C_{Lmin}E_L(T_5 - T_{L1}) \quad (20)$$

The heat leakages between the heat source and the environment [127,128] are neglected. Therefore, the W and η are:

$$W = \dot{Q}_{2-3} + \dot{Q}_{3-4} - \dot{Q}_{5-1} \quad (21)$$

$$\eta = W / (\dot{Q}_{2-3} + \dot{Q}_{3-4}) \quad (22)$$

The dimensionless power output (\bar{W}) is:

$$\bar{W} = W / (C_{wf}T_0) \quad (23)$$

The maximum specific volume corresponding to state point 5 is v_5 . The P is calculated as:

$$P = W / v_5 \quad (24)$$

The specific volume corresponding to state point 1 is v_1 . The dimensionless power density (\bar{P}) and dimensionless maximum specific volume (v_5/v_1) are obtained as:

$$\bar{P} = \frac{P}{C_{wf}T_0/v_1} = \frac{W/v_5}{C_{wf}T_0/v_1} = \frac{W}{C_{wf}T_0} \times \frac{T_1}{T_5} = \bar{W} \times \frac{T_1}{T_5} \quad (25)$$

$$v_5/v_1 = T_5/T_1 \quad (26)$$

There are two different methods for calculating the entropy production rate. One was suggested by Bejan [129,130], and the another was suggested by Salamon et al. [131]. In this article, the method used is the one suggested by the latter.

The entropy production rate (s_g) and E are, respectively, calculated as:

$$s_g = C_H \ln(T_{H2}/T_{H1}) + C_{H1} \ln(T_{H4}/T_{H3}) + C_L \ln(T_{L2}/T_{L1}) \quad (27)$$

$$E = W - T_0 s_g \quad (28)$$

The dimensionless ecological function (\bar{E}) is obtained as:

$$\bar{E} = E / (C_{wf} T_0) \tag{29}$$

Equations (10)–(12) and (16)–(29) are combined, and the four dimensionless performance indicators of the cycle are obtained as follows:

$$\bar{W} = \frac{C_{wf}xy(C_{H1}E_{H1}T_{H3} + C_{Lmin}E_L T_{L1}) + C_{Hmin}E_H T_{H1} \left\{ xy[C_{wf} - C_{H1}E_{H1} + C_{Lmin}E_L(\eta_t - 1)] - C_{Lmin}E_L\eta_t \right\} + a_1 \left\{ C_{Lmin}E_L \times [(\eta_t - 1)xy - \eta_t](C_{wf} - E_H C_{Hmin}) - xy[C_{wf}C_{Hmin}E_H + C_{H1}E_{H1}(C_{wf} - C_{Hmin}E_H)] \right\}}{C_{wf}^2 T_0 xy} \tag{30}$$

$$\eta = \frac{C_{Hmin}C_{Lmin}E_H E_L \eta_t T_{H1} - \left\{ C_{Hmin}E_H T_{H1}[C_{wf} - C_{H1}E_{H1} + C_{Lmin}E_L(\eta_t - 1)] + C_{wf}xy(C_{H1}E_{H1}T_{H3} + C_{Lmin}E_L T_{L1}) \right\} + a_1 \left\{ [C_{Hmin}C_{wf}E_H + C_{H1}E_{H1}(C_{wf} - E_H C_{Hmin})]xy - C_{Lmin}E_L(C_{wf} - C_{Hmin}E_H)[(\eta_t - 1)xy - \eta_t] \right\}}{xy \left\{ a_1 [C_{H1}C_{wf}E_{H1} + C_{Hmin}E_H(C_{wf} - C_{H1}E_{H1})] + C_{Hmin}E_H(C_{H1}E_{H1} - C_{wf})T_{H1} - C_{H1}C_{wf}E_{H1}T_{H3} \right\}}$$

$$\bar{P} = \frac{\left\{ a_1(C_{wf} - C_{Hmin}E_H)(C_{wf} - C_{Lmin}E_L)[xy(\eta_t - 1) - \eta_t] - C_{Lmin}C_{wf}E_L T_{L1}xy + E_H C_{Hmin}T_{H1}(C_{wf} - C_{Lmin}E_L)[(\eta_t - 1)xy - \eta_t] \right\} \left\{ C_{wf}xy(C_{H1}E_{H1}T_{H3} + C_{Lmin}E_L T_{L1}) + \left\{ xy[C_{wf} - C_{H1}E_{H1} + C_{Lmin}E_L(\eta_t - 1)] - C_{Lmin}E_L\eta_t \right\} C_{Hmin} \times E_H T_{H1} + a_1 \left\{ C_{Lmin}(C_{wf} - E_H C_{Hmin})E_L \left\{ (\eta_t - 1)xy - \eta_t - xy[C_{Hmin}C_{wf}E_H + C_{H1}E_{H1}(C_{wf} - C_{Hmin}E_H)] \right\} \right\} \right\}}{C_{wf}^3 T_0 xy [a_1(C_{wf} - C_{Hmin}E_H) + C_{Hmin}E_H T_{H1}][(\eta_t - 1)xy - \eta_t]} \tag{32}$$

$$\bar{E} = \frac{\left\{ C_{wf}xy(C_{H1}E_{H1}T_{H3} + C_{Lmin}E_L T_{L1}) + C_{Hmin}E_H T_{H1} \left\{ xy[C_{wf} - C_{H1}E_{H1} + C_{Lmin}E_L(\eta_t - 1)] - C_{Lmin}E_L\eta_t \right\} + a_1 \left\{ C_{Lmin}E_L(C_{wf} - C_{Hmin}E_H)[(\eta_t - 1)xy - \eta_t] - xy[C_{wf}C_{Hmin}E_H + C_{H1}E_{H1}(C_{wf} - C_{Hmin}E_H)] \right\} \right\} / (T_0 \times xy) - C_{wf} \left\{ C_L \ln \left\{ 1 + \left\{ C_{Lmin}E_L \left\{ a_1 C_{wf}\eta_t - C_{wf}xy[a_1(\eta_t - 1) + T_{L1}] + C_{Hmin}E_H(a_1 - T_{H1})[(\eta_t - 1)xy - \eta_t] \right\} \right\} / (C_L C_{wf} T_{L1} xy) \right\} + C_H \ln \left\{ a_1 \times C_{Hmin}E_H + (C_H - C_{Hmin}E_H)T_{H1} / (C_H T_{H1}) \right\} + C_{H1} \ln \left\{ 1 + \left\{ E_{H1}[C_{wf} \times (a_1 - T_{H3}) + E_H C_{Hmin}(T_{H1} - a_1)] \right\} / (C_{wf} T_{H3}) \right\} \right\}}{C_{wf}^2}$$

where

$$a_1 = \frac{(\eta_c + x - 1) \left\{ C_{Lmin}C_{wf}E_L T_{L1}xy - C_{Hmin}E_H T_{H1}(C_{wf} - C_{Lmin}E_L)[(\eta_t - 1)xy - \eta_t] \right\}}{C_{Hmin}C_{Lmin}E_H E_L(\eta_c + x - 1)(\eta_t xy - xy - \eta_t) + C_{wf}^2 [xy - x^2 y + \eta_t(\eta_c + x - 1)(xy - 1)] - C_{wf}(\eta_c + x - 1)(E_H C_{Hmin} + E_L C_{Lmin})[(\eta_t - 1)xy - \eta_t]} \tag{34}$$

Parameters x and y in Equations (30)–(34) can be obtained by Equations (13) and (19), and then the arithmetic solution of \bar{W} , η , \bar{P} and \bar{E} can be gained. When C_H , C_{H1} , C_L , E_H , E_{H1} , E_L , η_c and η_t are specific values, the cycle could be transformed into different cycle models. Equations (30)–(34) could be simplified into the performance indicators of the various cycle models, which have certain universality.

1. When $C_{H1} = C_L \rightarrow \infty$, Equations (30)–(34) can be simplified into the performance indicators of the irreversible simple BCY with an IHP and coupled to constant-temperature heat reservoirs (CTHRs) whose $T - s$ diagram is shown in Figure 3a:

$$\bar{W} = \frac{C_{wf}xy(C_{H1}E_{H1}T_{H3} + C_{Lmin}E_L T_{L1}) + C_{Hmin}E_H T_{H1} \left\{ xy[C_{wf} - C_{H1}E_{H1} + C_{Lmin}E_L(\eta_t - 1)] - C_{Lmin}E_L\eta_t \right\} + a_1 \left\{ C_{Lmin}E_L \times [(\eta_t - 1)xy - \eta_t](C_{wf} - E_H C_{Hmin}) - xy[C_{wf}C_{Hmin}E_H + C_{H1}E_{H1}(C_{wf} - C_{Hmin}E_H)] \right\}}{C_{wf}^2 T_0 xy} \tag{35}$$

$$\eta = \frac{C_{wf}E_H E_L \eta_t T_{H1} - \left\{ E_H T_{H1} [C_{wf} - C_{H1}E_{H1} + C_{wf}E_L(\eta_t - 1)] + (C_{H1}E_{H1}T_{H3} + C_{wf}E_L T_{L1}) \right\} xy + a_2 \left\{ [C_{wf}E_H + C_{H1}E_{H1}(1 - E_H)]xy - C_{wf}E_L(1 - E_H) \times [-\eta_t + (-1 + \eta_t)xy] \right\}}{xy \left\{ a_2 [C_{H1}E_{H1} + E_H(C_{wf} - C_{H1}E_{H1})] + E_H T_{H1} (C_{H1}E_{H1} - C_{wf}) - C_{H1}E_{H1}T_{H3} \right\}} \tag{36}$$

$$\bar{P} = \frac{C_{wf} \left\{ -E_L T_{L1} xy + a_2(1 - E_H)(1 - E_L)[(\eta_t - 1)xy - \eta_t] + E_H T_{H1}(1 - E_L)[(\eta_t - 1)xy - \eta_t] \right\} \left\{ xy(C_{H1}E_{H1}T_{H3} + C_{wf}E_L T_{L1}) + E_H T_{H1} \left\{ xy[C_{wf} - C_{H1}E_{H1} + C_{wf} \times E_L(\eta_t - 1)] - C_{wf}E_L\eta_t \right\} + a_2 C_{wf}(1 - E_H)E_L \left\{ (\eta_t - 1)xy - \eta_t - C_{wf}xy[C_{wf}E_H + C_{H1}E_{H1}(1 - E_H)] \right\} \right\}}{C_{wf}^3 T_0 xy [a_2(1 - E_H) + E_H T_{H1}][(\eta_t - 1)xy - \eta_t]} \tag{37}$$

$$\bar{E} = \frac{\left\{ xy(C_{H1}E_{H1}T_{H3} + C_{wf}E_L T_{L1}) + E_H T_{H1} \left\{ [C_{wf} - C_{H1}E_{H1} + C_{wf}E_L(\eta_t - 1)]xy - E_L\eta_t \right\} + a_2 C_{wf} \left\{ C_{wf}E_L(1 - E_H)[(\eta_t - 1)xy - \eta_t] - xy[C_{wf}E_H + C_{H1}(1 - E_H)E_{H1}] \right\} \right\} / (T_0 xy) - \left\{ C_H \ln[(a_2 C_{wf}E_H + C_H T_{H1} - C_{wf}E_H T_{H1}) / (C_H T_{H1})] + C_{H1} \ln \left\{ 1 + \left\{ E_{H1} [a_2 + C_{wf}E_H \times (T_{H1} - a_2) / C_{wf} - T_{H3}] \right\} / T_{H3} \right\} + C_L \ln \left\{ 1 + \left\{ C_{wf}E_L \{ a_2 \eta_t - xy [a_2(\eta_t - 1) + T_{L1}] + E_H \times (a_2 - T_{H1}) [(\eta_t - 1)xy - \eta_t] \} \right\} / (C_L T_{L1} xy) \right\} \right\}}{C_{wf}} \tag{38}$$

where

$$a_2 = \frac{(\eta_c + x - 1) \left\{ -E_L T_{L1} xy - E_H T_{H1}(1 - E_L)[(\eta_t - 1)xy - \eta_t] \right\}}{E_H E_L (\eta_c + x - 1) [(xy - 1)\eta_t - xy] + [xy - x^2 y + \eta_t(\eta_c + x - 1) \times (xy - 1)] - [(\eta_t - 1)xy - \eta_t](\eta_c + x - 1)(E_H + E_L)} \tag{39}$$

2. When $\eta_{c1} = \eta_{t1} = 1$, Equations (30)–(34) can be respectively simplified into the performance indicators of the endoreversible simple BCY with an IHP and coupled to VTNRs [99], whose $T - s$ diagram is shown in Figure 3b:

$$\bar{W} = \frac{C_{wf}x \left\{ C_{Lmin}C_{wf}E_L T_{L1}(y - 1) + C_{H1}E_{H1} [C_{wf}T_{H3}(y - 1) + C_{Lmin}E_L(T_{H3} - T_{L1}xy)] \right\} + E_H C_{Hmin} \left\{ C_{Lmin}E_L [C_{wf}T_{H1}(x - 1) + C_{wf}T_{L1}x(1 - xy)] + C_{H1} \times E_{H1}x(T_{L1}xy - T_{H3}) \right\} + xC_{wf}[(y - 1)C_{wf}T_{H1} + C_{H1}E_{H1}(T_{H3} - T_{H1}y)] \right\}}{C_{wf}T_0 x [C_{wf}^2 y - (C_{wf} - C_{Hmin}E_H)(C_{wf} - C_{Lmin}E_L)]} \tag{40}$$

$$\eta = \frac{C_{wf}T_0 x \left\{ C_{Lmin}C_{wf}E_L T_{L1}(y - 1) + C_{H1}E_{H1} [C_{wf}T_{H3}(y - 1) + C_{Lmin}E_L(T_{H3} - T_{L1}xy)] \right\} + C_{Hmin}E_H \left\{ C_{Lmin}E_L [C_{wf}T_{H1}(x - 1) + C_{wf}T_{L1}x(1 - xy)] + C_{H1}E_{H1}x(T_{L1}xy - T_{H3}) \right\} + C_{wf}x [C_{wf}T_{H1}(y - 1) + C_{H1}E_{H1}(T_{H3} - T_{H1}y)] \right\}}{C_{wf}T_0 x \left\{ C_{Hmin}E_H [C_{wf}^2 T_{H1}(y - 1) + C_{H1}C_{wf}E_{H1}(T_{H3} - T_{H1}y)] + C_{Lmin}C_{wf}E_L(T_{H1} - T_{L1}xy) + C_{H1}C_{Lmin}E_{H1}E_L(T_{L1}xy - T_{H3}) \right\} + C_{H1}C_{wf}E_{H1} [C_{wf}T_{H3}(y - 1) + C_{Lmin}E_L(T_{H3} - T_{L1}xy)] \right\}} \tag{41}$$

$$\bar{P} = \frac{[C_{Hmin}E_H T_{H1}(C_{wf} - C_{Lmin}E_L) + C_{Lmin}C_{wf}E_L T_{L1}xy] \{C_{wf}x \{C_{Lmin}C_{wf}E_L T_{L1}(y - 1) + C_{H1}E_{H1} \times [C_{wf}T_{H3}(y - 1) + C_{Lmin}E_L(T_{H3} - T_{L1}xy)]\} + C_{Hmin}E_H \{C_{wf}x[C_{wf}T_{H1}(y - 1) + (T_{H3} - T_{H1} \times y)C_{H1}E_{H1}] + C_{Lmin}E_L[C_{wf}T_{H1}(x - 1) + C_{wf}T_{L1}x(1 - xy) + C_{H1}E_{H1}x(T_{L1}xy - T_{H3})]\}}}{C_{wf}T_0x[C_{wf}^2y - (C_{wf} - C_{Hmin}E_H)(C_{wf} - C_{Lmin}E_L)][C_{Lmin}(C_{wf} - C_{Hmin}E_H)E_L \times T_{L1}x + C_{Hmin}C_{wf}E_H T_{H1}]} \quad (42)$$

$$\bar{E} = \frac{C_{wf}x \{C_{Lmin}C_{wf}E_L T_{L1}(y - 1) + C_{H1}E_{H1}[C_{wf}T_{H3}(y - 1) + C_{Lmin}E_L(T_{H3} - T_{L1}xy)]\} + C_{Hmin}E_H \{C_{Lmin}E_L[C_{wf}T_{H1}(x - 1) + C_{wf}T_{L1}x(1 - xy) + C_{H1} \times E_{H1}x(T_{L1}xy - T_{H3})] + C_{wf}x[C_{wf}T_{H1}(y - 1) + (T_{H3} - T_{H1}y)C_{H1}E_{H1}]\}}{C_{wf}T_0x[C_{wf}^2y - (C_{wf} - C_{Hmin}E_H)(C_{wf} - C_{Lmin}E_L)]} \quad (43)$$

$$- \frac{C_H}{C_{wf}T_0} \ln \left\{ 1 + \frac{C_{Hmin}C_{wf}E_H(C_{wf}T_{H1} - C_{Lmin}E_L T_{H1} - C_{wf}T_{H1}y + C_{Lmin} \times E_L T_{L1}xy)}{T_{H1}[C_H C_{wf}^2y - C_H(C_{wf} - C_{Hmin}E_H)(C_{wf} - C_{Lmin}E_L)]} \right\}$$

$$- \frac{C_{H1}}{C_{wf}T_0} \ln \frac{\{ (C_{wf} - C_{Hmin}E_H)(E_{H1} - 1)(C_{wf} - C_{Lmin}E_L)T_{H3} + C_{wf}y \times [C_{Hmin}E_H E_{H1} T_{H1} - C_{wf}(E_{H1} - 1)T_{H3}] + C_{Lmin}E_{H1}E_L T_{L1}xy \times (C_{wf} - C_{Hmin}E_H) \}}{C_{wf}^2 T_{H3}y - T_{H3}(C_{wf} - C_{Hmin}E_H)(C_{wf} - C_{Lmin}E_L)}$$

$$- \frac{C_L}{C_{wf}T_0} \ln \left\{ 1 + \frac{C_{Lmin}C_{wf}E_L[C_{Hmin}E_H(T_{H1} - T_{L1}x) - C_{wf}T_{L1}x(y - 1)]}{C_L T_{L1}[(C_{Hmin}E_H - C_{wf})(C_{wf}C_{Lmin}E_L)x + C_{wf}^2xy]} \right\}$$

3. When $\eta_{c1} = \eta_{t1} = 1$ and $C_{H1} = C_{H2} = C_L \rightarrow \infty$, Equations (30)–(34) can be simplified into the performance indicators of the endoreversible simple BCY with an IHP and coupled to CTHR, whose $T - s$ diagram is shown in Figure 3c:

$$\bar{W} = \frac{C_{wf}x \{C_{wf}E_L T_{L1}(y - 1) + C_{H1}E_{H1}[E_L T_{H3} - E_L T_{L1}xy + T_{H3}(y - 1)]\} + C_{wf}E_H \{E_L [T_{H1}C_{wf}(x - 1) + C_{wf}T_{L1}x(1 - xy) + C_{H1}E_{H1}x(T_{L1}xy - T_{H3})] + x[C_{wf}T_{H1}(y - 1) + C_{H1}E_{H1}(T_{H3} - T_{H1}y)]\}}{C_{wf}^2 T_0x(E_H + E_L + y - E_H E_L - 1)} \quad (44)$$

$$\eta = \frac{T_0x \{C_{wf}E_L T_{L1}y - C_{wf}E_L T_{L1} + C_{H1}E_{H1}[T_{H3}y - T_{H3} + T_{H3}E_L - E_L T_{L1}xy]\} + \{E_H \{x[C_{wf}T_{H1}y - C_{wf}T_{H1} + C_{H1}E_{H1}(T_{H3} - T_{H1}y)] + E_L [C_{wf}T_{H1}x - C_{wf} \times T_{H1} + C_{wf}T_{L1}x(1 - xy) + C_{H1}E_{H1}x(-T_{H3} + T_{L1}xy)]\}}}{C_{wf}T_0x \{ [C_{wf}T_{H1}y - C_{wf}T_{H1} + C_{H1}E_{H1}(T_{H3} - T_{H1}y) + C_{wf}E_L(T_{H1} - T_{L1}xy) + C_{H1}E_{H1}E_L(T_{L1}xy - T_{H3})]E_H + C_{H1}E_{H1}[T_{H3}(y - 1) + E_L(T_{H3} - T_{L1}xy)]\}} \quad (45)$$

$$\bar{P} = \frac{[E_H T_{H1}(1 - E_L) + E_L T_{L1}xy] \{C_{wf}x \{C_{wf}E_L T_{L1}(y - 1) + C_{H1}E_{H1}[T_{H3}(y - 1) + E_L(T_{H3} - T_{L1}xy)]\} + E_H C_{wf} \{x[C_{wf}T_{H1}(y - 1) + C_{H1}E_{H1}(T_{H3} - T_{H1}y)] + E_L [C_{wf}T_{H1}(x - 1) + C_{wf}T_{L1}x(1 - xy) + C_{H1}x E_{H1}(T_{L1}xy - T_{H3})]\}}}{C_{wf}^2 T_0x(E_H + E_L + y - E_H E_L - 1)(E_H T_{H1} + E_L T_{L1}x - E_L T_{L1}x E_H)} \quad (46)$$

$$\bar{E} = \frac{\left\{ C_{wf} E_L T_{L1} (y - 1) + C_{H1} E_{H1} [T_{H3} (y - 1) + E_L T_{H3} T_{L1} x y] \right\} x + E_H \left\{ E_L [C_{wf} T_{H1} (x - 1) + (1 - x y) C_{wf} T_{L1} x + C_{H1} E_{H1} x (T_{L1} \times x y - T_{H3})] + x [C_{wf} T_{H1} (y - 1) + C_{H1} E_{H1} (T_{H3} - T_{H1} y)] \right\}}{C_{wf} T_0 x y - C_{wf} T_0 x (1 - E_H - E_L + E_H E_L) - \frac{C_{wf} T_{H3} (1 - E_H - E_L + E_H E_L) (E_{H1} - 1) + C_{wf} \times y [E_H E_{H1} T_{H1} - T_{H3} (E_{H1} - 1)] + E_{H1} E_L T_{L1} x y \times (1 - E_H)}{C_{wf} T_0} \ln \frac{C_{wf} [T_{H3} y - T_{H3} (1 - E_H) (1 - E_L)]}{E_H C_{wf} (T_{H1} - E_L \times T_{H1} - T_{H1} y + E_L T_{L1} x y)} - \frac{C_H}{C_{wf} T_0} \ln \left\{ 1 + \frac{E_H C_{wf} (T_{H1} - E_L \times T_{H1} - T_{H1} y + E_L T_{L1} x y)}{T_{H1} C_H [y - (1 - E_H) (1 - E_L)]} \right\} - \frac{C_L}{C_{wf} T_0} \ln \left\{ 1 + \frac{E_L C_{wf} [E_H (T_{H1} - T_{L1} x) - T_{L1} x (y - 1)]}{C_L T_{L1} [(E_H - 1) (1 - E_L) x + x y]} \right\}} \quad (47)$$

4. When $E_{H1} = 0$, Equations (30)–(34) can be simplified into the performance indicators of the simple irreversible BCY coupled to VTHERs [79], whose $T - s$ diagram is shown in Figure 3d:

$$\bar{W} = \frac{C_{Lmin} C_{wf} E_L T_{L1} x + C_{Hmin} E_H T_{H1} \left\{ C_{Lmin} E_L [\eta_t (x - 1) - x] + C_{wf} x \right\} + a_3 \left\{ C_{Lmin} (C_{wf} - C_{Hmin} E_H) E_L [\eta_t (x - 1) - x] - C_{Hmin} C_{wf} E_H x \right\}}{C_{wf}^2 T_0 x} \quad (48)$$

$$\eta = \frac{a_3 \left\{ C_{Hmin} C_{wf} E_H x - C_{Lmin} E_L (C_{wf} - C_{Hmin} E_H) [\eta_t (x - 1) - x] \right\} - C_{Lmin} \times C_{wf} E_L T_{L1} x + C_{Hmin} E_H T_{H1} [C_{Lmin} E_L (\eta_t + x - \eta_t x) - C_{wf} x]}{x C_{Hmin} E_H C_{wf} (a_3 - T_{H1})} \quad (49)$$

$$\bar{P} = \frac{\left\{ -a_3 [\eta_t (x - 1) - x] (C_{wf} - C_{Hmin} E_H) (C_{wf} - C_{Lmin} E_L) - C_{Hmin} E_H T_{H1} [\eta_t (x - 1) - x] \times (C_{wf} - C_{Lmin} E_L) + C_{Lmin} C_{wf} E_L T_{L1} x \right\} \left\{ a_3 \left\{ C_{Lmin} E_L [\eta_t (x - 1) - x] (C_{wf} - C_{Hmin} E_H) - C_{Hmin} C_{wf} E_H x \right\} + C_{Hmin} E_H T_{H1} \left\{ C_{Lmin} E_L [\eta_t (x - 1) - x] + C_{wf} x \right\} + C_{Lmin} C_{wf} E_L T_{L1} x \right\}}{-C_{wf}^3 T_0 x [\eta_t (x - 1) - x] [a_3 (C_{wf} - C_{Hmin} E_H) + C_{Hmin} E_H T_{H1}]} \quad (50)$$

$$\bar{E} = \frac{\left\{ C_{Lmin} C_{wf} E_L T_{L1} x + C_{Hmin} E_H T_{H1} \left\{ C_{Lmin} E_L [\eta_t (x - 1) - x] + C_{wf} x \right\} + a_3 \left\{ C_{Lmin} (C_{wf} - C_{Hmin} E_H) E_L [\eta_t (x - 1) - x] - C_{Hmin} C_{wf} E_H x \right\} \right\} / (T_0 x) - C_{wf} \left\{ C_H \ln [1 + C_{Hmin} E_H \times (a_3 - T_{H1}) / (C_H T_{H1})] + C_L \ln \left\{ 1 + C_{Lmin} E_L \left\{ a_3 C_{wf} \eta_t + C_{Hmin} E_H (a_3 - T_{H1}) [\eta_t (x - 1) - x] - C_{wf} [a_3 (\eta_t - 1) + T_{L1}] x \right\} / (C_L C_{wf} T_{L1} x) \right\} \right\}}{C_{wf}^2} \quad (51)$$

where

$$a_3 = \frac{(\eta_c + x - 1) \left\{ C_{Lmin} C_{wf} E_L T_{L1} x - C_{Hmin} E_H T_{H1} (C_{wf} - C_{Lmin} E_L) [(\eta_t - 1) x - \eta_t] \right\}}{C_{Hmin} C_{Lmin} E_H E_L (\eta_c + x - 1) (\eta_t x - x - \eta_t) + C_{wf}^2 [x - x^2 + \eta_t (\eta_c + x - 1) (x - 1)] - C_{wf} (\eta_c + x - 1) (E_H C_{Hmin} + E_L C_{Lmin}) \times [(\eta_t - 1) x - \eta_t]} \quad (52)$$

5. When $E_{H1} = 0$ and $C_H = C_L \rightarrow \infty$, Equations (30)–(34) can be simplified into the performance indicators of the simple irreversible BCY coupled to CTHR [76], whose $T - s$ diagram is shown in Figure 3e:

$$\bar{W} = \frac{E_L T_{L1} x - a_4 \left\{ (E_H - 1) E_L [\eta_t (x - 1) - x] + E_H x \right\} + E_H T_{H1} [E_L \eta_t (x - 1) + x - E_L x]}{T_0 x} \quad (53)$$

$$\eta = \frac{a_4(E_H - 1)E_L[\eta_t(x - 1) - x] + a_4E_Hx - E_H T_{H1}x - E_L T_{L1}x + E_H E_L T_{H1}(\eta_t + x - \eta_t x)}{x E_H (a_4 - T_{H1})} \tag{54}$$

$$\bar{P} = \frac{\{a_4(E_H - 1)(E_L - 1)[\eta_t(x - 1) - x] - E_H T_{H1}(E_L - 1)[\eta_t(x - 1) - x] - E_L T_{L1}x\} \{a_4(E_H - 1)E_L[\eta_t(x - 1) - x] + a_4E_Hx - E_H T_{H1}x - E_L T_{L1}x + E_H E_L T_{H1}(\eta_t + x - \eta_t x)\}}{T_0[a_4(E_H - 1) - E_H T_{H1}][\eta_t(x - 1) - x]x} \tag{55}$$

$$\bar{E} = \frac{\{E_L T_{L1}x - a_4\{E_L(E_H - 1)[\eta_t(x - 1) - x] + E_Hx\} + E_H T_{H1}[E_L \eta_t(x - 1) + x - E_Lx]\} / (T_0x) - C_H \ln[1 + C_{wf} E_H (a_4 - T_{H1}) / (C_H T_{H1})] / C_{wf} - C_L \ln\{1 + C_{wf} E_L \{a_4(E_H - 1)[\eta_t(x - 1) - x] - T_{L1}x + E_H T_{H1}(\eta_t + x - \eta_t x)\} / (C_L T_{L1}x)\} / C_{wf}}{\quad} \tag{56}$$

where

$$a_4 = \frac{(\eta_c + x - 1)E_H T_{H1}(E_L - 1)[\eta_t(x - 1) - x] + E_L T_{L1}x}{(E_H - 1)(E_L - 1)(x - 1)(\eta_c + x - 1)\eta_t - x[x - 1 + E_H(E_L - 1)(\eta_c + x - 1) - E_L(\eta_c + x - 1)]} \tag{57}$$

- 6. When $E_{H1} = 0$ and $\eta_c = \eta_t = 1$, Equations (30)–(34) can be simplified into the performance indicators of the simple endoreversible BCY coupled to VTHRs [78], whose $T - s$ diagram is shown in Figure 3f:

$$\bar{W} = \frac{C_{Hmin} C_{Lmin} E_H E_L (-1 + x)(T_{H1} - T_{L1}x)}{T_0 x [C_{Lmin} C_{wf} E_L + C_{Hmin} E_H (C_{wf} - C_{Lmin} E_L)]} \tag{58}$$

$$\eta = (x - 1) / x \tag{59}$$

$$\bar{P} = \frac{C_{Hmin} C_{Lmin} E_H E_L (-1 + x)(T_{H1} - T_{L1}x) [C_{Hmin} E_H (C_{wf} - C_{Lmin} E_L) T_{H1} + C_{Lmin} C_{wf} E_L T_{L1}x]}{T_0 x [C_{Lmin} C_{wf} E_L + C_{Hmin} E_H (C_{wf} - C_{Lmin} E_L)] [C_{Lmin} C_{wf} \times E_L T_{L1}x + C_{Hmin} E_H (C_{wf} T_{H1} - C_{Lmin} E_L T_{L1}x)]} \tag{60}$$

$$\bar{E} = \frac{\frac{C_{Hmin} C_{Lmin} C_{wf} E_H E_L (x - 1)(T_{H1} - T_{L1}x)}{[C_{Lmin} C_{wf} E_L + C_{Hmin} E_H (C_{wf} - C_{Lmin} E_L)] T_0 x} - C_H \ln\left[1 + \frac{C_{Hmin} C_{Lmin} C_{wf} E_H E_L (T_{L1}x - T_{H1})}{C_H [C_{Lmin} C_{wf} E_L + C_{Hmin} E_H (C_{wf} - C_{Lmin} E_L)] T_{H1}}\right] - C_L \ln\left\{\frac{C_L C_{Lmin} C_{wf} E_L T_{L1}x + C_{Hmin} E_H [C_L C_{wf} T_{L1}x + C_{Lmin} E_L (C_{wf} T_{H1} - C_L T_{L1}x - C_{wf} T_{L1}x)]}{C_L [C_{Lmin} C_{wf} E_L + C_{Hmin} E_H (C_{wf} - C_{Lmin} E_L)] T_{L1}x}\right\}}{C_{wf}} \tag{61}$$

- 7. When $E_{H1} = 0$, $\eta_c = \eta_t = 1$ and $C_H = C_L \rightarrow \infty$, Equations (30)–(34) can be simplified into the performance indicators of the simple endoreversible BCY coupled to CTHRs [77], whose $T - s$ diagram is shown in Figure 3g:

$$\bar{W} = \frac{E_H E_L (-1 + x)(T_{L1}x - T_{H1})}{[E_H(E_L - 1) - E_L] T_0 x} \tag{62}$$

$$\eta = (x - 1) / x \tag{63}$$

$$\bar{P} = \frac{E_H E_L (x - 1)(T_{L1}x - T_{H1}) [E_H(E_L - 1) T_{H1} - E_L T_{L1}x]}{T_0 x (E_H E_L T_{L1}x - E_H T_{H1} - E_L T_{L1}x) [E_H(E_L - 1) - E_L]} \tag{64}$$

$$\bar{E} = \frac{C_{wf} E_H E_L (x - 1)(T_{L1}x - T_{H1}) + C_H T_0 x (E_H + E_L - E_H E_L) \ln\{1 - C_{wf} E_H \times E_L (T_{H1} - T_{L1}x) / [C_H T_{H1} (E_H + E_L - E_H E_L)]\} + C_L T_0 x (E_H + E_L - E_H \times E_L) \ln[1 + C_{wf} E_H E_L (T_{H1} - T_{L1}x) / (C_L (E_H + E_L - E_H E_L) T_{L1}x)]}{C_{wf} [E_H(E_L - 1) - E_L] T_0 x} \tag{65}$$

8. When $E_H = E_L = 0, \eta_c = \eta_t = 1$ and $C_{wf} \rightarrow \infty$, the cycle in this paper can become the endoreversible Carnot cycle coupled to VTHRs [14], whose $T - s$ diagram is shown in Figure 3h. However, Equations (30), (33), and (34) need to be de-dimensionalized to simplify to W, P and E of the endoreversible Carnot cycle coupled to VTHRs. The performance indicators of the cycle are:

$$W = \frac{C_H C_L E_H E_L (x - 1) (T_{H1} - T_{L1} x)}{x (C_H E_H + C_L E_L)} \tag{66}$$

$$\eta = (x - 1) / x \tag{67}$$

$$P = \frac{C_H C_L E_H E_L (x - 1) (T_{H1} - T_{L1} x)}{x (C_H E_H + C_L E_L)} \tag{68}$$

$$E = \frac{C_H C_L E_H E_L (x - 1) (T_{H1} - T_{L1} x)}{(C_H E_H + C_L E_L) x} - C_H T_0 \ln \left[1 + \frac{C_L E_H E_L (T_{L1} x - T_{H1})}{(C_H E_H + C_L E_L) T_{H1}} \right] - C_L T_0 \ln \left[\frac{C_H E_H E_L T_{H1} + C_H E_H T_{L1} x + C_L E_L T_{L1} x - C_H E_H E_L T_{L1} x}{C_H E_H T_{L1} x + C_L E_L T_{L1} x} \right] \tag{69}$$

9. When $E_H = E_L = 0, \eta_c = \eta_t = 1$ and $C_{H1} = C_L = C_{wf} \rightarrow \infty$, the cycle in this paper can become the endoreversible Carnot cycle coupled to CTHRs [12], whose $T - s$ diagram is shown in Figure 3i. However, Equations (30), (33), and (34) also need to be de-dimensionalized to simplify to W, P and E of the cycle [12,74,82]. The performance indicators of the cycle are:

$$W = \frac{U_H U_L (-1 + x) (T_{H1} - T_{L1} x)}{(U_H + U_L) x} \tag{70}$$

$$\eta = (x - 1) / x \tag{71}$$

$$P = \frac{U_H U_L (-1 + x) (T_{H1} - T_{L1} x)}{(U_H + U_L) x} \tag{72}$$

$$E = \frac{U_H U_L (T_{H1} - T_{L1} x) [(T_0 + T_{H1}) T_{L1} x - T_{H1} (T_0 + T_{L1})]}{T_{H1} T_{L1} (U_H + U_L) x} \tag{73}$$

10. When $E_H = E_L = 0, \eta_c = \eta_t = 1, C_{H1} = C_L = C_{wf} \rightarrow \infty$, and $U_L \rightarrow \infty$, the cycle in this paper can become the endoreversible Novikov cycle coupled to CTHRs [11], whose $T - s$ diagram is shown in Figure 3j. However, Equations (30), (33), and (34) also need to be de-dimensionalized to simplify to W, P and E of the cycle [11]. The performance indicators of the cycle are:

$$W = \frac{U_H (x - 1) (T_{H1} - T_{L1} x)}{x} \tag{74}$$

$$\eta = (x - 1) / x \tag{75}$$

$$P = \frac{U_H (x - 1) (T_{H1} - T_{L1} x)}{x} \tag{76}$$

$$E = \frac{U_H (T_{H1} - T_{L1} x) [T_{H1} T_{L1} (x - 1) + T_0 (T_{L1} x - T_{H1})]}{T_{H1} T_{L1} x} \tag{77}$$

11. Through comparison with the results in Refs [11–14,59,76–79,99], it is found that the results of this paper are consistent with those in Refs [11–14,59,76–79,99], which further illustrates the accuracy of the model established in this paper. In particular, when the powers in Equations (58), (62), (66), (70), and (74) take the maximum values, namely $x = \sqrt{T_{H1}/T_{L1}}$, the efficiencies at the maximum power point, Equations (59), (63), (67), (71), and (75) are $\eta = 1 - \sqrt{T_{L1}/T_{H1}}$, which was derived in Refs. [10–12] by Moutier [10], Novikov [11], and Curzon and Ahlborn [12]. One can see that the results of this paper include the Novikov–Curzon–Ahlborn efficiency.
12. FTT is the further extension of conventional irreversible thermodynamics. The cycle model established by Curzon and Ahlborn [12] was a reciprocating Carnot cycle, and the finite time was its major feature. The methods used for solving the FTT problem are usually variational principle and optimal control theory. Therefore, such problems of extremal of thermodynamic processes were first named as FTT by Andresen et al. [132] and as Optimization Thermodynamics or Optimal Control in Problems of Extremals of Irreversible Thermodynamic Processes by Orlov and Rudenko [133]. When the research object was extended from reciprocating devices characterized by finite-time to the steady state flow devices characterized by finite-size, one realizes that the physical property of the problems is the heat transfer owing to temperature difference. Therefore, Grazzini [14] termed it Finite Temperature Difference Thermodynamics, and Lu [134] termed it Finite Surface Thermodynamics. In fact, the works performed by Moutier [10] and Novikov [11] were also steady state flow device models. Bejan introduced the effect of temperature difference heat transfer on the total entropy generation of the systems, taking the entropy generation minimization as the optimization objective for designing thermodynamic processes and devices, termed “Entropy Generation Minimization” or “Thermodynamic Optimization” [15,135]. For the steady state flow device models, Feidt [136–146] termed it Finite Physical Dimensions Thermodynamics (FPDT). The model established herein is closer to FPDT. For both reciprocating model and steady state flow model, the suitable name may be thermodynamics of finite size devices and finite time processes, as Bejan termed it [15,135]. According to the idiomatic usage, the theory is termed FTT in this paper.

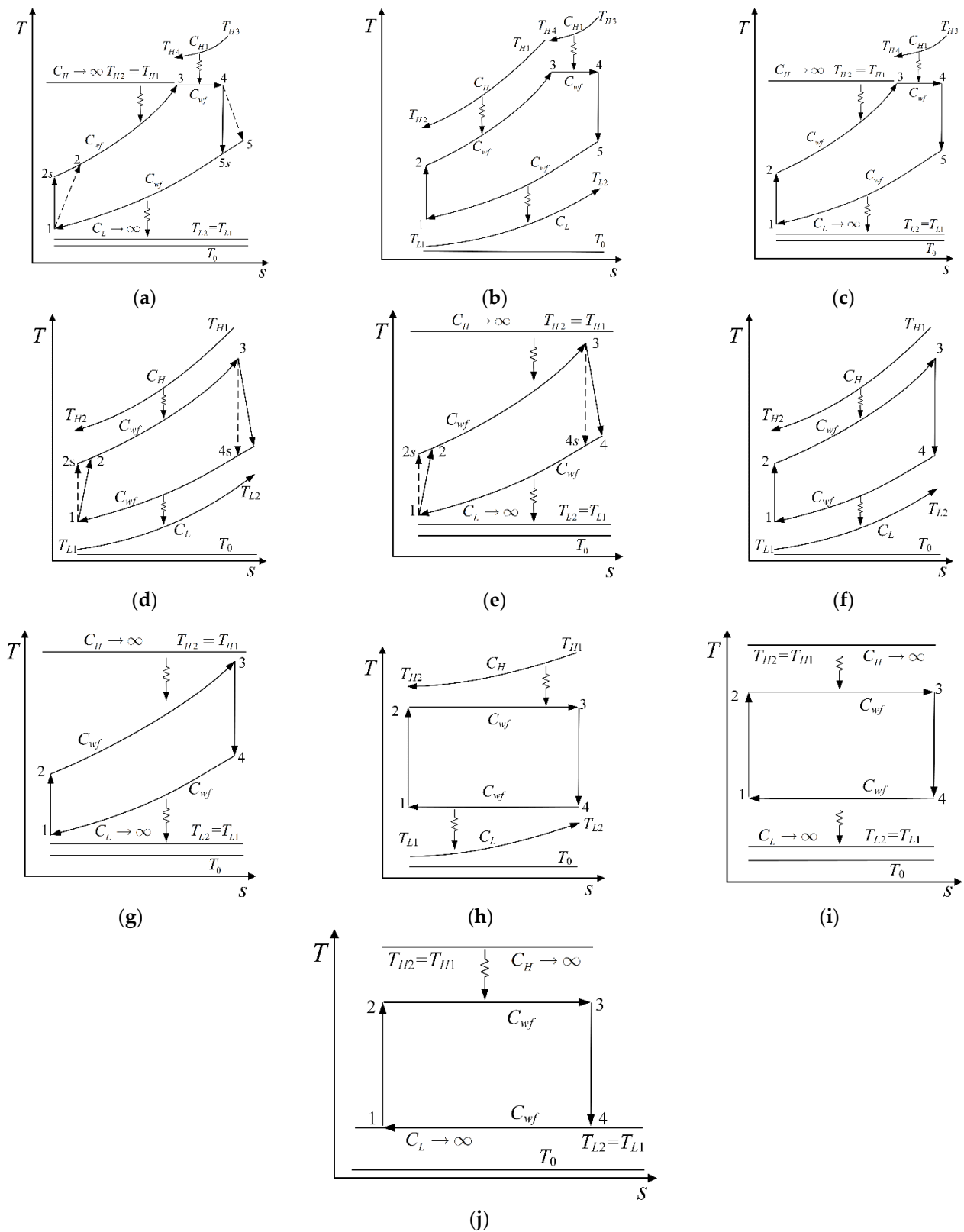


Figure 3. Diagrams of (a) irreversible simple BCY with an IHP and coupled to CTHRs; (b) endoreversible simple BCY with an IHP and coupled to VTHRs; (c) endoreversible simple BCY with an IHP and coupled to CTHRs; (d) simple irreversible BCY coupled to VTHRs; (e) simple irreversible BCY coupled to CTHRs; (f) simple endoreversible BCY coupled to VTHRs; (g) simple endoreversible BCY coupled to CTHRs; (h) endoreversible Carnot cycle coupled to VTHRs; (i) endoreversible Carnot cycle coupled to CTHRs; (j) endoreversible Novikov cycle coupled to CTHRs.

3. Analyses and Optimizations with Each Single Objective

3.1. Analyses of Each Single Objective

The impacts of the irreversibility on cycle performance indicators (\bar{W} , η , \bar{P} and \bar{E}) are analyzed below. In numerical calculations, it is set that $C_L = C_H = 1.2$ kW/K, $C_{wf} = 1$ kW/K, $T_0 = 300$ K, $C_{H1} = 0.6$ kW/K, $k = 1.4$, $R_g = 0.287$ kJ/(kg · K), $E_H = E_{H1} = E_L = 0.9$, $C_p = 1.005$ kW/K, $\tau_{H1} = 4.33$, $\tau_{H3} = 5$ and $\tau_L = 1$.

Figures 4–6 present the relationships of \bar{W} , η , \bar{P} , \bar{E} , π_t and v_5/v_1 versus π with different η_t . As shown in Figures 4 and 5, \bar{W} , η , \bar{P} and \bar{E} increase and then decrease as π increases. In the same situation, \bar{W} , \bar{E} , \bar{P} and η reach the maximum value successively. When $\eta_t = 0.7$ and $\pi = 32.3$, $\bar{W} = \bar{P} = 0$. If π keeps going up, \bar{W} and \bar{P} are going to go negative. \bar{W} , η , \bar{P} and \bar{E} increase as η_t increases. As π increases, \bar{W} , η , \bar{P} and \bar{E} are affected more significantly by η_t . As shown in Figure 6, π_t goes up but v_5/v_1 goes down as π goes up. π_t and v_5/v_1 decrease as η_t rises. It illustrates that the degree of the IHP is improved and the device's volume is reduced as η_t increases.

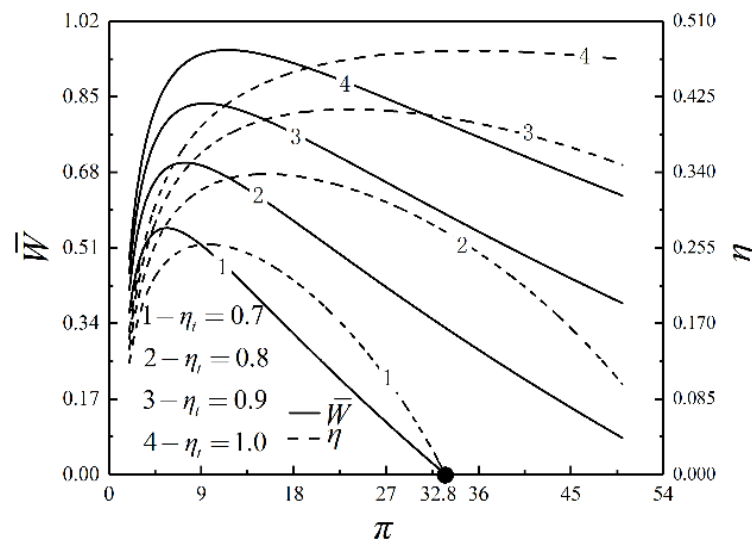


Figure 4. Relationships of \bar{W} and η versus π with different η_t .

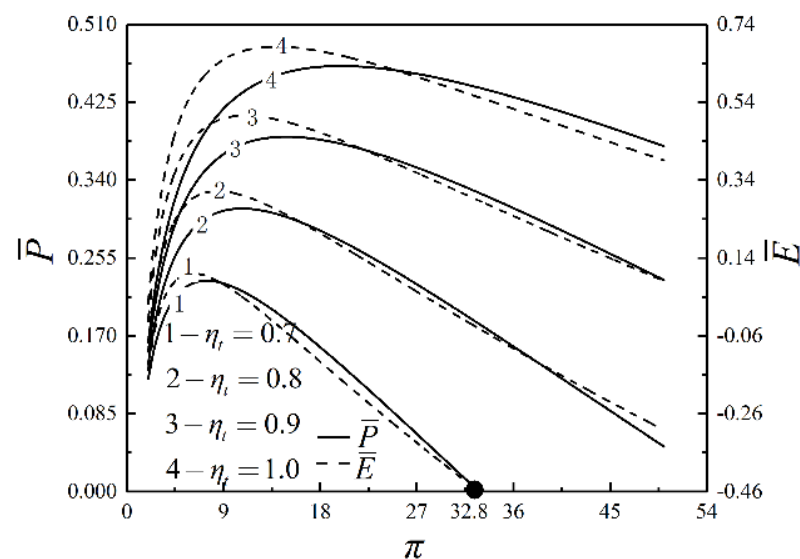


Figure 5. Relationships of \bar{P} and \bar{E} versus π with different η_t .

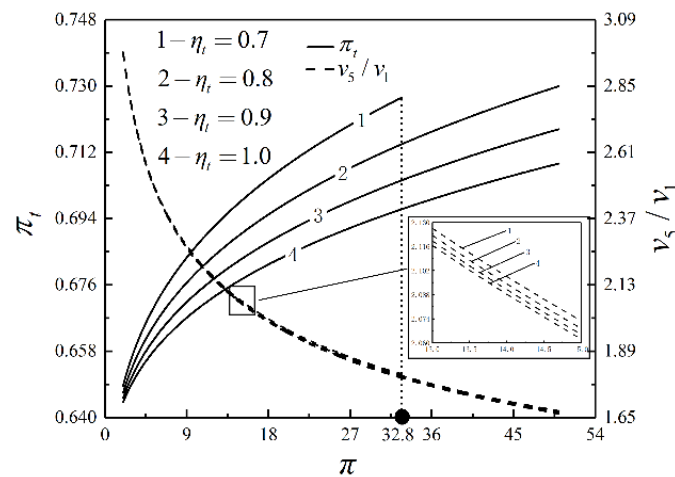


Figure 6. Relationships of π_t and v_5/v_1 versus π with different η_t .

By numerical calculations, the influences of η_c on \bar{W} , η , \bar{P} , \bar{E} and π_t are the same as those of η_t on \bar{W} , η , \bar{P} , \bar{E} and π_t . When $\eta_t = 0.7$ and $\pi = 32.8$, $\bar{W} = \bar{P} = 0$. However, the impacts of η_c on \bar{W} , η , \bar{P} and \bar{E} are less than those of η_t on \bar{W} ,

η , \bar{P} , \bar{E} . The effect of η_c on π_t is more significant than that of η_t on π_t . η_c has little effect on v_5/v_1 . In the actual design process, it is suggested that η_t should be given priority.

To further explain the difference between the models in this paper and Ref. [101], the comparison of \bar{W} under the variable and constant π is shown in Figure 7. As shown in Figure 7, \bar{W} increases and then decreases as π increases in both cases; that is, the qualitative law is the same. However, there is an apparent quantitative difference between the two points. Under the constant π , \bar{W} corresponding to the constant π is always greater than \bar{W} conforming to the variable π . Similarly, there are quantitative differences in η , \bar{P} and \bar{E} under the variable and constant π . The model whose π is variable is more realistic.

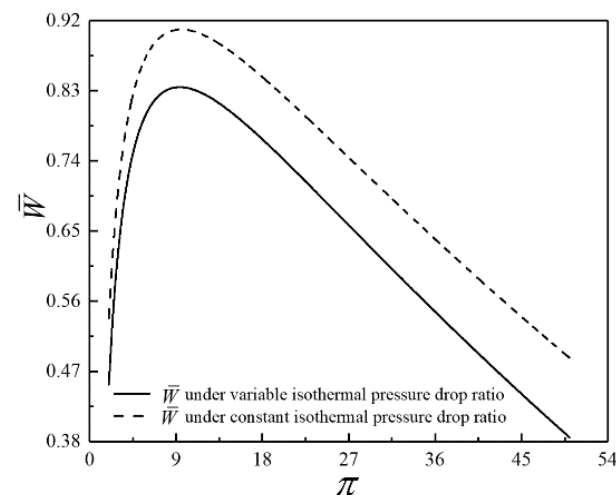


Figure 7. Comparison of \bar{W} under the variable and constant π .

3.2. Performance Optimizations for Each Single Objective

With four performance indicators as the OPOs, respectively, the HCDs are optimized under the condition of given total heat conductance (U_T). The optimal results under different OPOs are compared. The HCDs among the RCC, CCC, and precooler are:

$$u_H = U_H/U_T, u_{H1} = U_{H1}/U_T, u_L = U_L/U_T \tag{78}$$

The HCDs are must larger than 0, the sum of them is 1, and $2 \leq \pi \leq 50$.

Figure 8 shows the flowchart of HCD optimization. The steps are as follows:

1. Enter the known data and the initial values of the HCDs.
2. The π_t is calculated according to Equation (13).
3. Judge whether the π_t and HCDs meet the constraints. If they are satisfied, perform step 4; if they are not satisfied, go back to step 1.
4. The performance indicator is solved.
5. Determine whether the inverse objective function is minimized by using the “fmincon” in MATLAB. If it is the smallest, perform step 6; if it is not the slightest, go back to step 1.
6. Calculate the other thermodynamic parameters, and the maximum of the performance indicator is obtained.

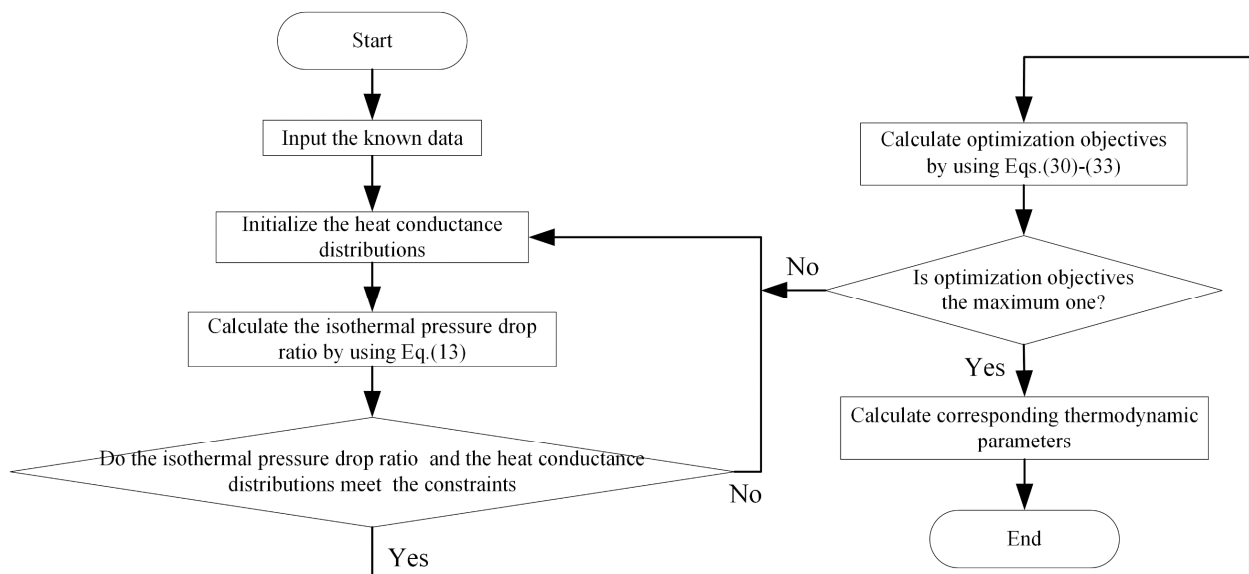


Figure 8. Flowchart of HCD optimization.

3.2.1. Optimizations of Each Single Objective

The optimization results of four performance indicators are similar. The optimization results with η as the performance indicator will be mainly discussed herein, while the results with \bar{W} , \bar{P} and \bar{E} as the performance indicators are briefly discussed. The relationships of the optimal thermal efficiency (η_{opt}) and the corresponding dimensionless power output ($\bar{W}_{\eta_{opt}}$) versus π are shown in Figure 9. The relationships of the corresponding dimensionless power density ($\bar{P}_{\eta_{opt}}$) and the corresponding dimensionless ecological function ($\bar{E}_{\eta_{opt}}$) versus π are demonstrated in Figure 10. As shown in Figures 9 and 10, $\bar{W}_{\eta_{opt}}$, η_{opt} , $\bar{P}_{\eta_{opt}}$ and $\bar{E}_{\eta_{opt}}$ first rise and then drops as π rises, which indicates a parabolic relationship with the downward opening. The corresponding isothermal pressure drop ratio ($(\pi_t)_{\eta_{opt}}$) and dimensionless maximum specific volume ($(v_5/v_1)_{\eta_{opt}}$) versus π are shown in Figure 11. $(\pi_t)_{\eta_{opt}}$ decreases and then increases as π increases. It indicates that there is a π_t that maximizes the degree of isothermal heating in the cycle. $(v_5/v_1)_{\eta_{opt}}$ decreases as π increases. The relationships of the HCDs ($(u_H)_{\eta_{opt}}$, $(u_{H1})_{\eta_{opt}}$ and $(u_L)_{\eta_{opt}}$) versus π are shown in Figure 12. As π increases, $(u_H)_{\eta_{opt}}$ decreases, $(u_{H1})_{\eta_{opt}}$ increases rapidly and then slowly, and $(u_L)_{\eta_{opt}}$ decreases first and then increases gradually.

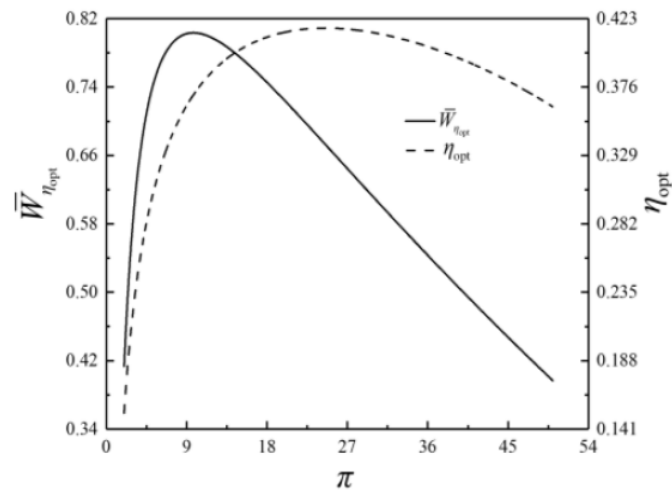


Figure 9. Relationships of $\bar{W}_{\eta_{opt}}$ and η_{opt} versus π .

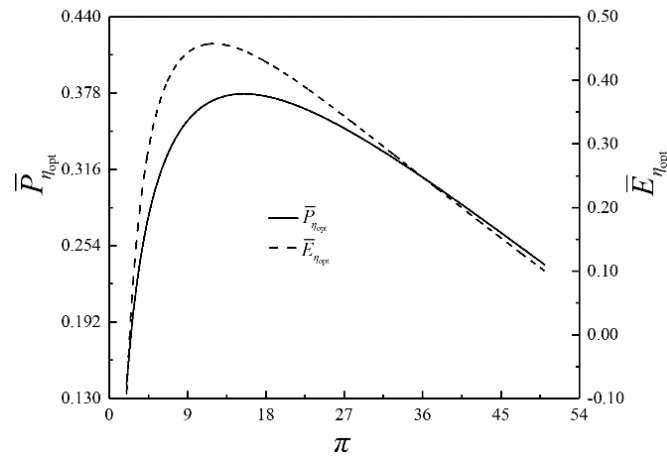


Figure 10. Relationships of $\bar{P}_{\eta_{opt}}$ and $\bar{E}_{\eta_{opt}}$ versus π .

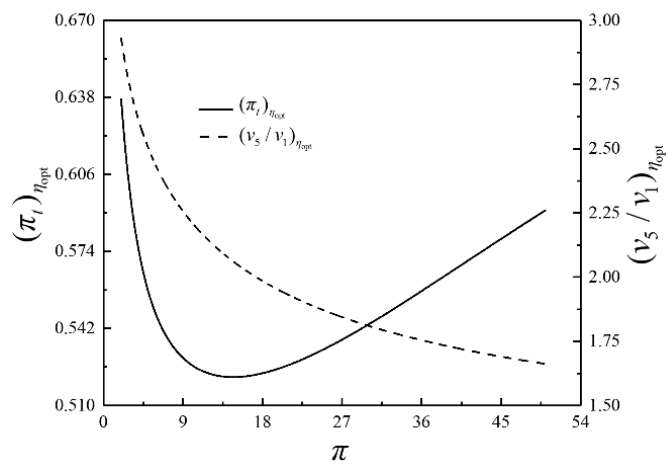


Figure 11. Relationships of $(\pi_t)_{\eta_{opt}}$ and $(v_5/v_1)_{\eta_{opt}}$ versus π .

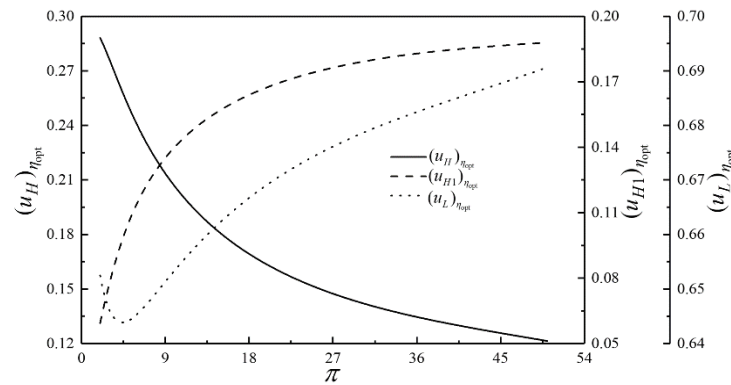


Figure 12. Relationships of $(u_H)_{\eta_{opt}}$, $(u_{H1})_{\eta_{opt}}$ and $(u_L)_{\eta_{opt}}$ versus π .

By numerical calculations, \bar{W}_{opt} , $\eta_{\bar{W}_{opt}}$, $\bar{P}_{\bar{W}_{opt}}$, $\bar{E}_{\bar{W}_{opt}}$, $\bar{W}_{\bar{P}_{opt}}$, $\eta_{\bar{P}_{opt}}$, \bar{P}_{opt} , $\bar{E}_{\bar{P}_{opt}}$, $\bar{W}_{\bar{E}_{opt}}$, $\eta_{\bar{E}_{opt}}$, $\bar{P}_{\bar{E}_{opt}}$ and \bar{E}_{opt} increase first and then decrease as π increases. As π increases, $(\pi_t)_{\bar{W}_{opt}}$, $(\pi_t)_{\bar{P}_{opt}}$ and $(\pi_t)_{\bar{E}_{opt}}$ reduce first and then increase, and $(\pi_t)_{\bar{W}_{opt}}$, $(\pi_t)_{\bar{E}_{opt}}$, $(\pi_t)_{\eta_{opt}}$ and $(\pi_t)_{\bar{P}_{opt}}$ reached the minimum successively. As π increases, $(v_5/v_1)_{\bar{W}_{opt}}$ and $(v_5/v_1)_{\bar{E}_{opt}}$ decline, and their values have little difference. $(u_H)_{\bar{W}_{opt}}$, $(u_H)_{\eta_{opt}}$, $(u_H)_{\bar{P}_{opt}}$ and $(u_H)_{\bar{E}_{opt}}$ decrease as π increases, and $(u_H)_{\eta_{opt}}$ is always the smallest. $(u_{H1})_{\bar{W}_{opt}}$ and $(u_{H1})_{\bar{E}_{opt}}$ rise firstly and then tend to keep constant as π rises. $(u_{H1})_{\bar{P}_{opt}}$ first increases then decreases and finally tends to stay stable as π rises. $(u_L)_{\bar{W}_{opt}}$, $(u_L)_{\bar{P}_{opt}}$ and $(u_L)_{\bar{E}_{opt}}$ first increase rapidly and then slowly as π increases.

3.2.2. Influences of Temperature Ratios on Optimization Results

With η as the performance indicator, the influences of the temperature ratios on the optimization results are discussed. The relationship of the maximum thermal efficiency (η_{max}) versus τ_{H1} and τ_{H3} is shown in Figure 13. According to Figure 12, the surface is divided into three parts by line $\tau_{H3} = \tau_{H1} + 0.27$ (the correlation coefficient is $r_1 = 0.9969$) and $\tau_{H3} = 1.2\tau_{H1} + 0.1$ (the correlation coefficient is $r_2 = 1.0000$). τ_{H1} has little influence on η_{max} . When $\tau_{H3} < 1.2\tau_{H1} + 0.1$, η_{max} increases as τ_{H3} increases; when $\tau_{H3} > 1.2\tau_{H1} + 0.1$, τ_{H3} has little impact on η_{max} . It is recommended to magnify τ_{H1} .

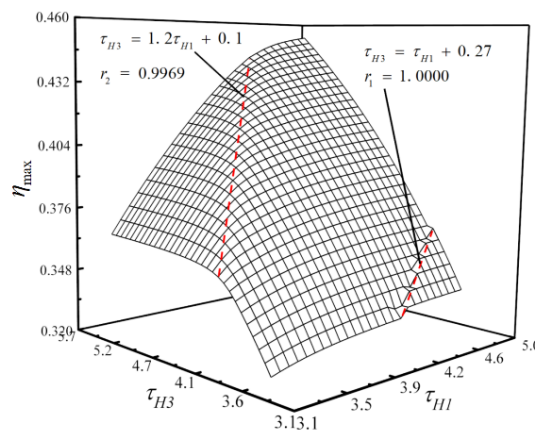


Figure 13. Relationships of η_{max} versus τ_{H1} and τ_{H3} .

By numerical calculations, the surface is divided into three parts by line $\tau_{H3} = 0.84\tau_{H1} + 0.41$ (the correlation coefficient is $r_1 = 0.9973$) and $\tau_{H3} = 1.2\tau_{H1} + 0.23$ (the correlation coefficient is $r_2 = 0.9988$) with \bar{W} as the performance indicator. The surface is divided into three parts by line $\tau_{H3} = 0.78\tau_{H1} + 0.6$ (the correlation coefficient is $r_1 = 0.9574$) and $\tau_{H3} = 1.2\tau_{H1} + 0.33$ (the correlation coefficient is $r_2 = 0.9991$) with \bar{P} as the

performance indicator. The surface is divided into three parts by line $\tau_{H3} = 0.93\tau_{H1} + 0.058$ (the correlation coefficient is $r_1 = 0.9978$) and $\tau_{H3} = 1.1\tau_{H1} + 0.41$ (the correlation coefficient is $r_2 = 0.9990$) with \bar{E} as the performance indicator. In practice, the difference between τ_{H1} and τ_{H3} should be controlled and should not be too large.

3.2.3. Influences of the Compressor and the Turbine’s Irreversibilities on Optimization Results

With the four performance indicators as OPOs, respectively, the influences of η_c and η_t on optimization results are considered, and the thermodynamic parameters under various optimal performance indicators are compared. Figures 14 and 15 show relationships of \bar{W} and π under various optimal performance indicators versus η_c and η_t , respectively. \bar{W}_{\max} , \bar{P}_{\max} , and \bar{E}_{\max} are the maximum dimensionless power output, maximum dimensionless power density, and maximum dimensionless ecological function, respectively. When \bar{W}_{\max} , η_{\max} , \bar{P}_{\max} , and \bar{E}_{\max} are used as subscripts, they indicate the corresponding values at \bar{W}_{\max} , η_{\max} , \bar{P}_{\max} , and \bar{E}_{\max} points.

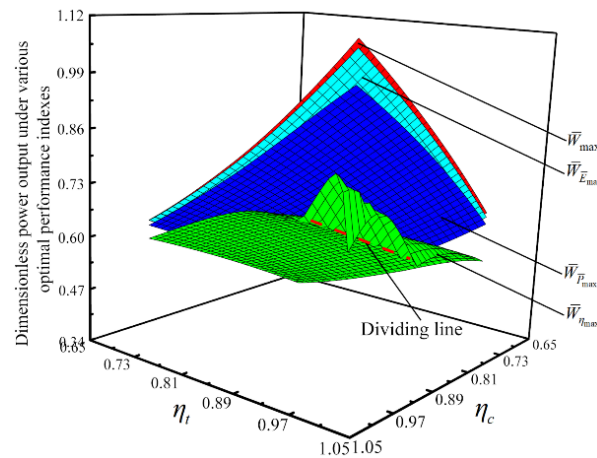


Figure 14. Relationships of \bar{W} under various optimal performance indexes versus η_c and η_t .

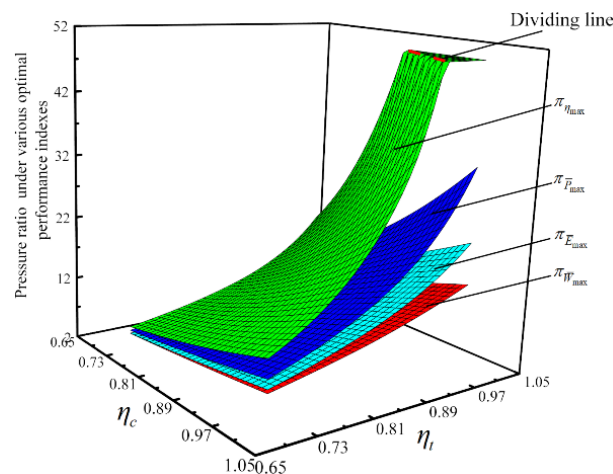


Figure 15. Relationships of π under various optimal performance indexes versus η_c and η_t .

As shown in Figure 14, \bar{W} under various optimal performance indicators increases as η_c or η_t increases. When η_c and η_t both approach 1, $\bar{W}_{\eta_{\max}}$ first increases and then decreases as η_c or η_t increases. When $\eta_c = \eta_t = 1$, η rises monotonically as π gains, and there is no maximum value. In the case of the same η_c and η_t , there is $\bar{W}_{\max} > \bar{W}_{\bar{E}_{\max}} > \bar{W}_{\bar{P}_{\max}} > \bar{W}_{\eta_{\max}}$. As shown in Figure 15, π under various optimal performance indicators all increase as η_c or η_t increases. But the influence of η_t on π is more significant than that of η_c on π .

When η_c and η_t both approach 1, $\pi_{\eta_{\max}}$ is always 50. Because the upper limit of π is 50. In the case of the same η_c and η_t , there is $\pi_{\eta_{\max}} > \pi_{\bar{P}_{\max}} > \pi_{\bar{E}_{\max}} > \pi_{\bar{W}_{\max}}$. The given range of π is $2 \leq \pi \leq 50$, so when $\pi = 50$, the trends of $\bar{W}_{\eta_{\max}}$ and $\pi_{\eta_{\max}}$ change significantly.

By numerical calculations, η , \bar{P} , and \bar{E} under various optimal performance indicators increases as η_c or η_t increases. When η_c and η_t both approach 1, $\bar{P}_{\eta_{\max}}$ and $\bar{E}_{\eta_{\max}}$ first rises and then drops as η_c or η_t rises. In the same η_c and η_t , there are $\eta_{\max} > \eta_{\bar{P}_{\max}} > \eta_{\bar{E}_{\max}} > \eta_{\bar{W}_{\max}}$, $\bar{P}_{\max} > \bar{P}_{\bar{E}_{\max}} > \bar{P}_{\bar{W}_{\max}} > \bar{P}_{\eta_{\max}}$, (when η_c and η_t both tend to 1, the relationship does not work) and $\bar{E}_{\max} > \bar{E}_{\bar{P}_{\max}} > \bar{E}_{\bar{W}_{\max}} > \bar{E}_{\eta_{\max}}$ (the difference between $\bar{E}_{\bar{P}_{\max}}$ and $\bar{E}_{\bar{W}_{\max}}$ is very small).

The calculations also show that the thermal capacitance rate matchings among the VTHRs and working fluid have influences on the cycle performance. \bar{W}_{\max} , η_{\max} , \bar{P}_{\max} , and \bar{E}_{\max} increase first and then keep constants as C_H/C_{wf} or C_{H1}/C_{wf} increases, and the effects of C_H/C_{wf} on \bar{W}_{\max} , η_{\max} , \bar{P}_{\max} , and \bar{E}_{\max} are more significant than that of C_{H1}/C_{wf} .

4. Multi-Objective Optimization

4.1. Optimization Algorithm and Decision-Making Methods

It is impossible to achieve the maximums of \bar{W} , η , \bar{P} , and \bar{E} under the same π . It shows that there is a contradiction among the four performance indicators. The multi-objective optimization problem is solved by applying the NSGA-II algorithm [99,100,102,105–125]. The detailed optimization process is shown in Figure 16. The Pareto frontier of the cycle performance is obtained by taking \bar{W} , η , \bar{P} , and \bar{E} as OPOs, using the NSGA-II algorithm. The optimal scheme is selected by using the LINMAP, TOPSIS, and Shannon Entropy methods [99,102], and the algorithm of “gamultiobj” in MATLAB is based on the NSGA-II algorithm. The calculations are assisted by applying the “gamultiobj”, and the corresponding Pareto frontier could be obtained. The parameter settings of “gamultiobj” are listed in Table 1.

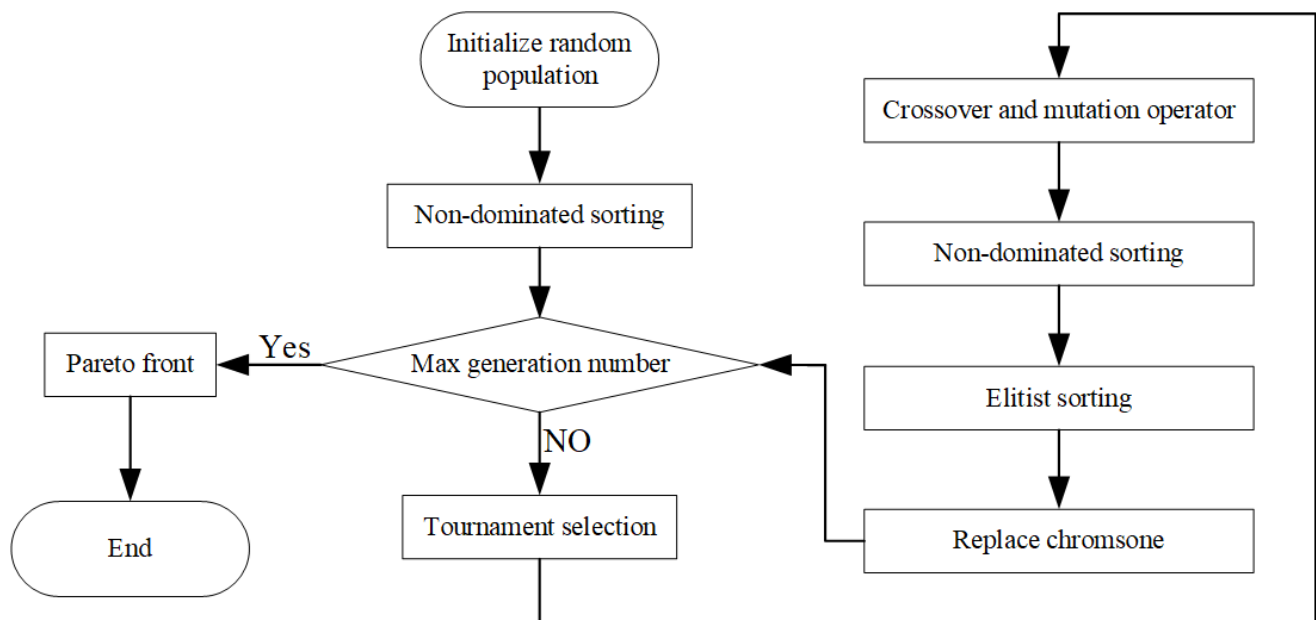


Figure 16. Flowchart of NSGA-II algorithm.

Table 1. Parameter settings of “gamultiobj”.

Parameters	Values
Nvars	4
ParetoFraction	0.3
PopulationSize	300
Generations	500
CrossoverFraction	0.8

The positive and negative ideal points are the optimal and inferior schemes of each performance indicator. The LINMAP method is the Euclidian distance between each scheme and the positive ideal point, among which the one with the smallest distance is the best scheme. Suppose that the Pareto front contains n feasible solutions, and each viable solution contains m objective values $F_{ij}(1 \leq i \leq m \text{ and } 1 \leq j \leq n)$. After normalizing F_{ij} , the value B_{ij} is:

$$B_{ij} = F_{ij} / \sqrt{\sum_{i=1}^n F_{ij}^2} \quad (79)$$

The weight of the j -th OPO is w_j^{LINMAP} , and the weighted value of B_{ij} is G_{ij} :

$$G_{ij} = w_j^{\text{LINMAP}} \cdot B_{ij} \quad (80)$$

The j -th objective of the positive ideal point is normalized and weighted, and the corresponding value is G_j^{positive} . The Euclidean distance between the i -th feasible solution and the positive ideal point is ED_i^+ :

$$ED_i^+ = \sqrt{\sum_{j=1}^m (G_{ij} - G_j^{\text{positive}})^2} \quad (81)$$

The best viable solution to the LINMAP method is i_{opt} :

$$i_{\text{opt}} \in \min\{ED_i^+\} \quad (82)$$

The TOPSIS method considers the Euclidean distance among each scheme and the positive and negative ideal points comprehensively, to further obtain the best scheme. The weight of the j -th OPO is w_j^{TOPSIS} , and the weighted value of B_{ij} is G_{ij} :

$$G_{ij} = w_j^{\text{TOPSIS}} \cdot B_{ij} \quad (83)$$

The j -th objective of the negative ideal point is normalized and weighted, and the corresponding value is G_j^{negative} . The Euclidean distance between the i -th feasible solution and the negative ideal point is ED_i^- :

$$ED_i^- = \sqrt{\sum_{j=1}^m (G_{ij} - G_j^{\text{negative}})^2} \quad (84)$$

The best feasible solution of the TOPSIS method is i_{opt} :

$$i_{\text{opt}} \in \min\left\{\frac{ED_i^-}{ED_i^+ + ED_i^-}\right\} \quad (85)$$

The Shannon Entropy method is a method to get the weight of multi-attribute decision-making.

After normalization of F_{ij} , P_{ij} is obtained:

$$P_{ij} = F_{ij} / \sum_{i=1}^n F_{ij} \tag{86}$$

The Shannon Entropy and weight of the j -th OPO are:

$$SE_j = -\frac{1}{\ln n} \sum_{i=1}^n P_{ij} \ln P_{ij} \tag{87}$$

$$w_j^{\text{Shannon Entropy}} = (1 - SE_j) / \sum_{j=1}^n (1 - SE_j) \tag{88}$$

The best feasible solution of the TOPSIS method is i_{opt} :

$$i_{\text{opt}} \in \min \left\{ P_{ij} \cdot w_j^{\text{Shannon Entropy}} \right\} \tag{89}$$

The deviation index D is defined as:

$$D = \frac{\sqrt{\sum_{j=1}^m (G_{i_{\text{opt}j}} - G_j^{\text{positive}})^2}}{\sqrt{\sum_{j=1}^m (G_{i_{\text{opt}j}} - G_j^{\text{positive}})^2} + \sqrt{\sum_{j=1}^m (G_{i_{\text{opt}j}} - G_j^{\text{negative}})^2}} \tag{90}$$

In this paper, $w_j^{\text{LINMAP}} = w_j^{\text{TOPSIS}} = 1$ is chosen for the convenience of calculation.

4.2. Multi-Objective Optimization Results

Figure 17 shows the Pareto frontier and optimal schemes corresponding to the four objectives (\bar{W} , η , \bar{P} and \bar{E}) optimization. The color on the Pareto frontier denotes the size of \bar{E} . To facilitate the observation of the changing relationships among the objectives, the pure red projection indicates the changing relationship between \bar{W} and η . The pure green projection shows the changing relationship between \bar{W} and \bar{P} , and the pure blue projection indicates the changing relationship between η and \bar{P} . It is easy to know that \bar{W} and η , \bar{W} and \bar{P} , η and \bar{P} are all parabolic-like relationships with the opening downward. To analyze the influence of the corresponding optimization variables ($(u_H)_{\text{opt}}$, $(u_{H1})_{\text{opt}}$, $(u_L)_{\text{opt}}$ and π_{opt}) on cycle performance, the distributions of $(u_H)_{\text{opt}}$, $(u_{H1})_{\text{opt}}$, $(u_L)_{\text{opt}}$ and π_{opt} within the Pareto frontier's value range are shown in Figures 18–21. As shown in Figure 18, the value range of $(u_H)_{\text{opt}}$ is 0–1, but its distribution is between 0.167 and 0.272. As $(u_H)_{\text{opt}}$ increases, \bar{W} , \bar{P} , and \bar{E} gradually increase, but η gradually decreases. As shown in Figure 19, the value range of $(u_{H1})_{\text{opt}}$ is 0–1, but its distribution is between 0.151 and 0.181. As $(u_{H1})_{\text{opt}}$ increases, \bar{W} , \bar{P} , and \bar{E} gradually decrease, but the changing trend of η is not apparent. As shown in Figure 20, the value range of $(u_L)_{\text{opt}}$ is 0–1, but its distribution is between 0.568 and 0.662. As $(u_L)_{\text{opt}}$ increases, \bar{W} , \bar{P} , and \bar{E} gradually decrease, but the changing trend of η is not apparent. As shown in Figure 21, the value range of π_{opt} is 2–50, but its distribution is between 9.692 and 24.426. As π_{opt} increases, \bar{W} gradually decreases, η gradually increases, and \bar{P} and \bar{E} rise and then reduce.

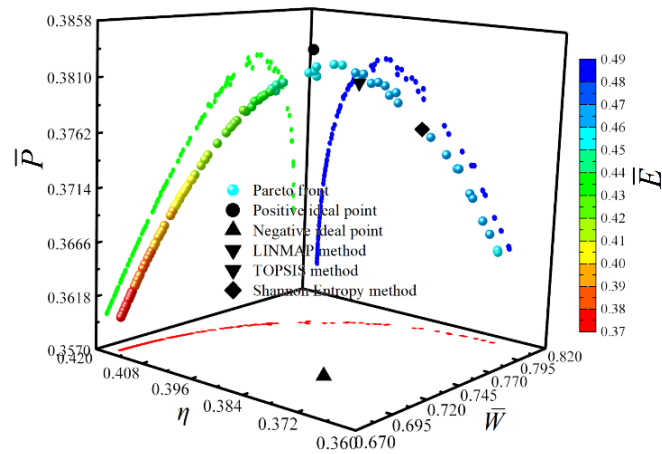


Figure 17. Pareto frontier and optimal schemes corresponding to the four objectives (\bar{W} , η , \bar{P} and \bar{E}) optimization.

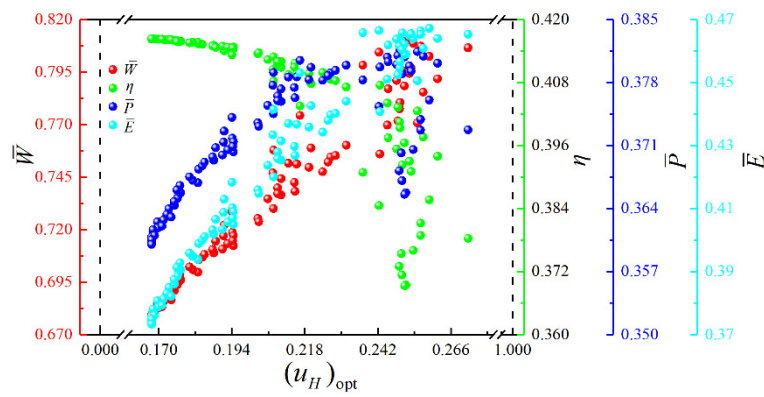


Figure 18. Distribution of $(u_H)_{opt}$ within the value range in the Pareto frontier.

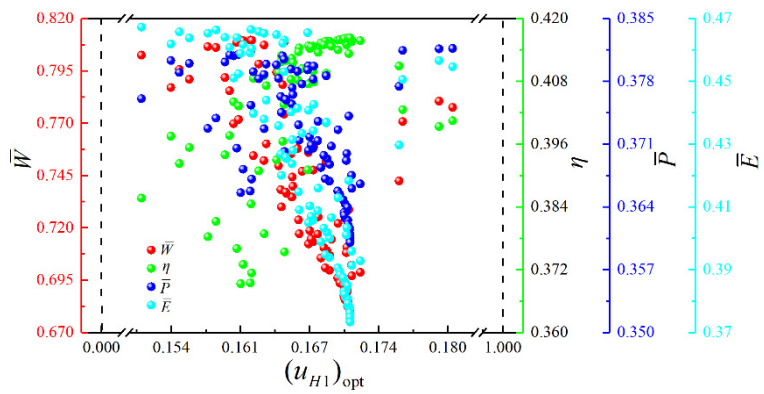


Figure 19. Distribution of $(u_{H1})_{opt}$ within the value range in the Pareto frontier.

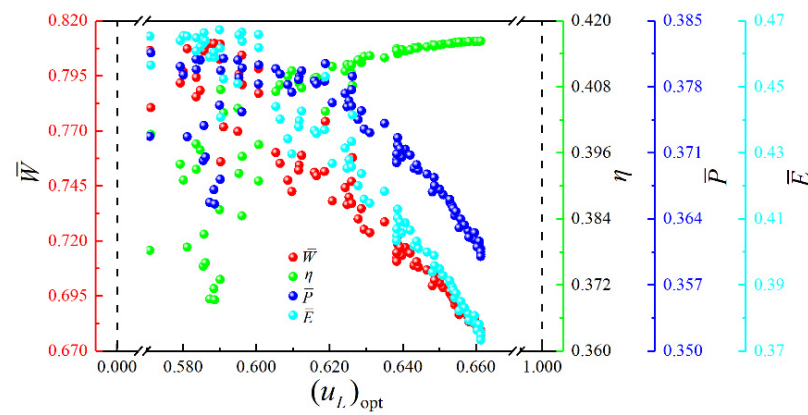


Figure 20. Distribution of $(u_L)_{opt}$ within the value range in the Pareto frontier.

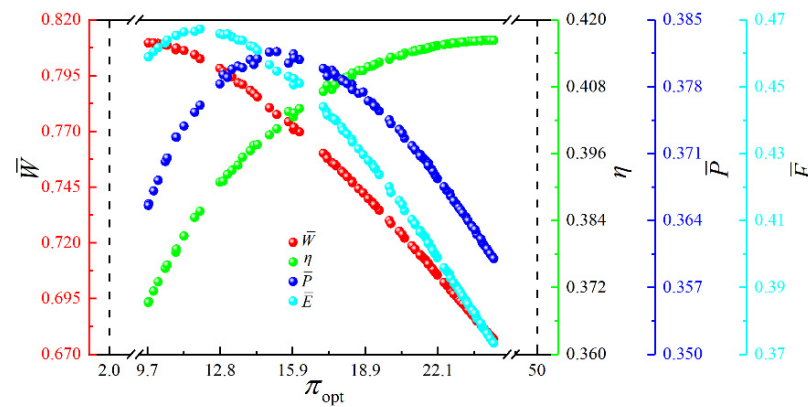


Figure 21. Distribution of π_{opt} within the value range in the Pareto frontier.

The Pareto frontier includes a series of non-inferior solutions, so the appropriate solution must be chosen according to the actual situation. The results of the triple- and double-objective optimizations are further discussed to compare the results of multi-objective optimizations more comprehensively. The comparison of the optimal schemes gotten by single- and double-, triple-, and quadruple-objective optimizations are listed in Table 2. The deviation index (D) is applied to represent the proximity between the optimal scheme and the positive ideal point. The appropriate optimal schemes are chosen by using the three methods. For the quadruple-objective optimization, \bar{W} , η , \bar{P} , and \bar{E} corresponding to the positive ideal point are the maximum of the single-objective optimization. It indicates that the Pareto frontier includes all single-objective optimization results. The D obtained by the Shannon Entropy method is significantly smaller than that obtained by the LINMAP and TOPSIS methods. Simultaneously, it can be found that the D obtained by the Shannon Entropy method is the same as that with \bar{E} as the OPO. For the triple-objective optimization, the triple-objective (\bar{W} , η and \bar{E}) optimization D obtained by the LINMAP or TOPSIS method is the smallest. For the double-objective optimization, the double-objective (\bar{W} and \bar{P}) optimization D obtained by the LINMAP method is the smallest. For the single-objective optimization, the D corresponding to \bar{E}_{max} is the smallest. For single- and double-, triple-, and quadruple-objective optimizations, the double-objective (\bar{W} and \bar{P}) optimization D obtained by the LINMAP method is the smallest.

Table 2. Comparison of the optimal schemes gotten by the single- and double-, triple-, and quadruple-objective optimizations.

OPOs	Decision Methods	Optimization Variables				Performance Indicators				Isothermal Pressure Drop Ratio	Deviation Indexes
		u_H	u_{H1}	u_L	π	\bar{W}	η	\bar{P}	\bar{E}	π_t	D
$\bar{W}, \eta, \bar{P},$ and \bar{E}	LINMAP	0.245	0.154	0.601	14.194	0.787	0.397	0.380	0.462	0.572	0.172
	TOPSIS	0.245	0.154	0.601	14.194	0.787	0.397	0.380	0.462	0.572	0.172
	Shannon Entropy	0.259	0.151	0.590	11.901	0.802	0.386	0.376	0.467	0.572	0.167
$\bar{W}, \eta,$ and \bar{P}	LINMAP	0.230	0.167	0.603	14.261	0.787	0.398	0.381	0.461	0.557	0.170
	TOPSIS	0.231	0.167	0.602	14.115	0.788	0.397	0.380	0.462	0.557	0.168
	Shannon Entropy	0.246	0.167	0.587	12.008	0.803	0.386	0.377	0.466	0.559	0.165
$\bar{W}, \eta,$ and \bar{E}	LINMAP	0.231	0.163	0.606	13.947	0.790	0.397	0.380	0.462	0.557	0.160
	TOPSIS	0.231	0.163	0.606	13.947	0.790	0.397	0.380	0.462	0.557	0.160
	Shannon Entropy	0.257	0.153	0.590	11.92	0.803	0.386	0.376	0.467	0.570	0.165
\bar{W}, \bar{P} and \bar{E}	LINMAP	0.252	0.177	0.571	13.339	0.793	0.393	0.380	0.463	0.566	0.162
	TOPSIS	0.252	0.177	0.571	13.339	0.793	0.393	0.380	0.463	0.566	0.162
	Shannon Entropy	0.259	0.151	0.590	11.906	0.802	0.386	0.376	0.467	0.572	0.167
η, \bar{P} and \bar{E}	LINMAP	0.241	0.170	0.589	17.016	0.761	0.406	0.380	0.444	0.575	0.319
	TOPSIS	0.241	0.170	0.589	17.016	0.761	0.406	0.380	0.444	0.575	0.319
	Shannon Entropy	0.245	0.169	0.585	16.674	0.764	0.405	0.381	0.447	0.577	0.297
\bar{W} and η	LINMAP	0.230	0.169	0.601	14.293	0.787	0.398	0.381	0.461	0.557	0.170
	TOPSIS	0.230	0.169	0.601	14.293	0.787	0.398	0.381	0.461	0.557	0.170
	Shannon Entropy	0.248	0.168	0.585	12.061	0.802	0.387	0.377	0.466	0.560	0.162
\bar{W} and \bar{P}	LINMAP	0.247	0.176	0.578	13.384	0.793	0.394	0.380	0.463	0.563	0.158
	TOPSIS	0.247	0.176	0.577	13.560	0.792	0.394	0.381	0.463	0.564	0.161
	Shannon Entropy	0.245	0.171	0.584	11.855	0.803	0.385	0.376	0.466	0.555	0.170
\bar{W} and \bar{E}	LINMAP	0.258	0.154	0.589	11.765	0.803	0.385	0.376	0.467	0.570	0.169
	TOPSIS	0.258	0.154	0.589	11.765	0.803	0.385	0.376	0.467	0.570	0.169
	Shannon Entropy	0.259	0.152	0.589	11.902	0.802	0.386	0.376	0.467	0.572	0.167
η and \bar{P}	LINMAP	0.232	0.192	0.576	16.452	0.765	0.405	0.381	0.446	0.562	0.295
	TOPSIS	0.235	0.193	0.572	16.156	0.768	0.404	0.381	0.447	0.563	0.279
	Shannon Entropy	0.241	0.196	0.563	15.603	0.772	0.402	0.381	0.450	0.564	0.255
η and \bar{E}	LINMAP	0.237	0.1604	0.603	14.307	0.787	0.398	0.381	0.461	0.564	0.170
	TOPSIS	0.236	0.163	0.601	14.173	0.788	0.398	0.381	0.462	0.562	0.164
	Shannon Entropy	0.258	0.152	0.590	11.909	0.802	0.386	0.376	0.467	0.571	0.167
\bar{P} and \bar{E}	LINMAP	0.257	0.166	0.578	13.483	0.792	0.394	0.380	0.464	0.572	0.160
	TOPSIS	0.257	0.165	0.578	13.386	0.793	0.393	0.380	0.464	0.572	0.161
	Shannon Entropy	0.258	0.154	0.588	12.054	0.802	0.387	0.377	0.467	0.571	0.161

Table 2. Cont.

OPOs	Decision Methods	Optimization Variables				Performance Indicators				Isothermal Pressure Drop Ratio	Deviation Indexes
		u_H	u_{H1}	u_L	π	\bar{W}	η	\bar{P}	\bar{E}	π_t	D
	\bar{W}	0.249	0.162	0.589	9.678	0.810	0.369	0.365	0.459	0.550	0.242
	η	0.152	0.174	0.674	24.542	0.672	0.416	0.358	0.369	0.532	0.783
	\bar{P}	0.251	0.183	0.567	15.149	0.777	0.400	0.382	0.454	0.571	0.225
	\bar{E}	0.259	0.151	0.590	11.903	0.802	0.386	0.376	0.467	0.572	0.167
	Positive ideal point	—	—	—	—	0.810	0.416	0.382	0.467	0.810	—
	Negative ideal point	—	—	—	—	0.677	0.369	0.360	0.373	0.677	—

5. Conclusions

Based on FTT, an improved irreversible closed modified simple BCY model with one IHP and coupled to VTHRs is established and optimized with four performance indicators as OPOs, respectively. The optimization results are compared, and the influences of compressor and turbine efficiencies on optimization results are analyzed. Finally, the cycle is optimized, and the corresponding Pareto frontier is gained by adopting the NSGA-II algorithm. Based on three different methods, the optimal scheme is gotten from the Pareto frontier. The results obtained in this paper reveal the original results in Refs. [10–12], which were the initial work of the FTT theory. The main results are summarized:

1. For the single-objective analyses and optimizations, performance indicators all rise as η_c and η_t rise. The influences of η_t on four performance indicators are greater than those of η_c . \bar{W} of the models in this paper increase and then decrease as π increases in both cases; that is, the qualitative law is the same. However, there is an apparent quantitative difference between the two points. In practice, the difference between τ_{H1} and τ_{H3} should be controlled and not be too large. \bar{P} and \bar{E} are the trade-offs between \bar{W} and η .
2. For single- and double-, triple-, and quadruple-objective optimizations, the Pareto frontier includes a series of non-inferior solutions. The appropriate solution could be chosen according to the actual situation. By comparison, it is found that the double-objective (\bar{W} and \bar{P}) optimization D obtained by the LINMAP method is the smallest.
3. The optimization results gained in this paper could offer theoretical guidelines for the optimal designs of the gas turbine plants. In the next step, the improved closed intercooling regenerated modified BCY model with one IHP will be optimized with real gas as the working fluid, and the internal friction-based pressure drops during heating and cooling processes and other processes, as well as the heat leakage losses between the heat source and the environment, will be taken into account.

Author Contributions: Conceptualization: L.C. and H.F.; funding acquisition: L.C.; methodology: C.T.; software: C.T. and Y.G.; validation: L.C. and Y.G.; writing—original draft: C.T. and H.F.; writing—review and editing: L.C. All authors have read and agreed to the published version of the manuscript.

Funding: This work is supported by the National Natural Science Foundation of China (Grant No. 51779262).

Acknowledgments: The authors wish to thank the reviewers for their careful, unbiased, and constructive suggestions, which led to this revised manuscript.

Conflicts of Interest: The authors declare no conflict of interest.

Nomenclature

a, x, y	Intermediate variables
C	Thermal capacity rate (kW/K)
C_p	Specific heat at constant pressure (kJ/(kg·K))
E	Effectiveness of heat exchanger or ecological function (kW)
\bar{E}	Dimensionless ecological function
k	Specific heat ratio
M	Mach number
N	Number of the heat transfer unit
\dot{Q}	Heat absorbing rate or heat releasing rate (kW)
\bar{P}	Dimensionless power density
T	Temperature (K)
U	Heat conductance (kW/K)
u	Heat conductance distribution

\bar{W} Dimensionless power output

Greek symbols

η Efficiency

π Pressure ratio

τ Temperature ratio

Subscripts

H Hot-side heat exchanger

L Cold-side heat exchanger

wf Working fluid

1, 2, 3, 4, 5, 2s, 5s State points

Abbreviations

Brayton cycle BCY

CCC Convergent combustion chamber

CTHR Constant-temperature heat reservoir

FPDT Finite Physical Dimensions Thermodynamics

FTT Finite time thermodynamics

HCD Heat conductance distribution

IHP Isothermal heating process

OPO Optimization objective

RCC Regular combustion chamber

VTHR Variable-temperature heat reservoir

References

- Wood, W.A. On the role of the harmonic mean isentropic exponent in the analysis of the closed-cycle gas turbine. *Proc. Inst. Mech. Eng. Part. A J. Power Energy* **1991**, *205*, 287–291. [[CrossRef](#)]
- Cheng, K.L.; Qin, J.; Sun, H.C.; Li, H.; He, S.; Zhang, S.L.; Bao, W. Power optimization and comparison between simple recuperated and recompressing supercritical carbon dioxide Closed-Brayton-Cycle with finite cold source on hypersonic vehicles. *Energy* **2019**, *181*, 1189–1201. [[CrossRef](#)]
- Hu, H.M.; Jiang, Y.Y.; Guo, C.H.; Liang, S.Q. Thermodynamic and exergy analysis of a S-CO₂ Brayton cycle with various of cooling modes. *Energy Convers. Manag.* **2020**, *220*, 113110. [[CrossRef](#)]
- Liu, H.Q.; Chi, Z.R.; Zang, S.S. Optimization of a closed Brayton cycle for space power systems. *Appl. Therm. Eng.* **2020**, *179*, 115611. [[CrossRef](#)]
- Vecchiarelli, J.; Kawall, J.G.; Wallace, J.S. Analysis of a concept for increasing the efficiency of a Brayton cycle via isothermal heat addition. *Int. J. Energy Res.* **1997**, *21*, 113–127. [[CrossRef](#)]
- Göktun, S.; Yavuz, H. Thermal efficiency of a regenerative Brayton cycle with isothermal heat addition. *Energy Convers. Manag.* **1999**, *40*, 1259–1266. [[CrossRef](#)]
- Erbay, L.B.; Göktun, S.; Yavuz, H. Optimal design of the regenerative gas turbine engine with isothermal heat addition. *Appl. Energy* **2001**, *68*, 249–264. [[CrossRef](#)]
- Jubeh, N.M. Exergy analysis and second law efficiency of a regenerative Brayton cycle with isothermal heat addition. *Entropy* **2005**, *7*, 172–187. [[CrossRef](#)]
- El-Maksoud, R.M.A. Binary Brayton cycle with two isothermal processes. *Energy Convers. Manag.* **2013**, *73*, 303–308. [[CrossRef](#)]
- Moutier, J. *Éléments de Thermodynamique*; Gautier-Villars: Paris, France, 1872.
- Novikov, I.I. The efficiency of atomic power stations (A review). *J. Nucl. Energy* **1957**, *7*, 125–128. [[CrossRef](#)]
- Curzon, F.L.; Ahlborn, B. Efficiency of a Carnot engine at maximum power output. *Am. J. Phys.* **1975**, *43*, 22–24. [[CrossRef](#)]
- Andresen, B. *Finite-Time Thermodynamics*; Physics Laboratory II; University of Copenhagen: Copenhagen, Denmark, 1983.
- Grazzini, G. Work from irreversible heat engines. *Energy* **1991**, *16*, 747–755. [[CrossRef](#)]
- Bejan, A. *Entropy Generation Minimization*; CRC Press: Boca Raton, FL, USA, 1996.
- Chen, L.G.; Wu, C.; Sun, F.R. Finite time thermodynamic optimization or entropy generation minimization of energy systems. *J. Non-Equilib. Thermodyn.* **1999**, *24*, 327–359. [[CrossRef](#)]
- Andresen, B. Current trends in finite-time thermodynamics. *Angew. Chem. Int. Ed.* **2011**, *50*, 2690–2704. [[CrossRef](#)] [[PubMed](#)]
- Shittu, S.; Li, G.Q.; Zhao, X.D.; Ma, X.L. Review of thermoelectric geometry and structure optimization for performance enhancement. *Appl. Energy* **2020**, *268*, 115075. [[CrossRef](#)]
- Berry, R.S.; Salamon, P.; Andresen, B. How it all began. *Entropy* **2020**, *22*, 908. [[CrossRef](#)] [[PubMed](#)]
- Hoffman, K.H.; Burzler, J.; Fischer, A.; Schaller, M.; Schubert, S. Optimal process paths for endoreversible systems. *J. Non-Equilib. Thermodyn.* **2003**, *28*, 233–268. [[CrossRef](#)]

21. Zaeva, M.A.; Tsirlin, A.M.; Didina, O.V. Finite time thermodynamics: Realizability domain of heat to work converters. *J. Non-Equilib. Thermodyn.* **2019**, *44*, 181–191. [[CrossRef](#)]
22. Masser, R.; Hoffmann, K.H. Endoreversible modeling of a hydraulic recuperation system. *Entropy* **2020**, *22*, 383. [[CrossRef](#)]
23. Kushner, A.; Lychagin, V.; Roop, M. Optimal thermodynamic processes for gases. *Entropy* **2020**, *22*, 448. [[CrossRef](#)]
24. De Vos, A. Endoreversible models for the thermodynamics of computing. *Entropy* **2020**, *22*, 660. [[CrossRef](#)] [[PubMed](#)]
25. Masser, R.; Khodja, A.; Scheunert, M.; Schwalbe, K.; Fischer, A.; Paul, R.; Hoffmann, K.H. Optimized piston motion for an alpha-type Stirling engine. *Entropy* **2020**, *22*, 700. [[CrossRef](#)] [[PubMed](#)]
26. Chen, L.G.; Ma, K.; Ge, Y.L.; Feng, H.J. Re-optimization of expansion work of a heated working fluid with generalized radiative heat transfer law. *Entropy* **2020**, *22*, 720. [[CrossRef](#)] [[PubMed](#)]
27. Tsirlin, A.; Gagarina, L. Finite-time thermodynamics in economics. *Entropy* **2020**, *22*, 891. [[CrossRef](#)] [[PubMed](#)]
28. Tsirlin, A.; Sukin, I. Averaged optimization and finite-time thermodynamics. *Entropy* **2020**, *22*, 912. [[CrossRef](#)]
29. Muschik, W.; Hoffmann, K.H. Modeling, simulation, and reconstruction of 2-reservoir heat-to-power processes in finite-time thermodynamics. *Entropy* **2020**, *22*, 997. [[CrossRef](#)] [[PubMed](#)]
30. Insinga, A.R. The quantum friction and optimal finite-time performance of the quantum Otto cycle. *Entropy* **2020**, *22*, 1060. [[CrossRef](#)]
31. Schön, J.C. Optimal control of hydrogen atom-like systems as thermodynamic engines in finite time. *Entropy* **2020**, *22*, 1066. [[CrossRef](#)]
32. Andresen, B.; Essex, C. Thermodynamics at very long time and space scales. *Entropy* **2020**, *22*, 1090. [[CrossRef](#)]
33. Chen, L.G.; Ma, K.; Feng, H.J.; Ge, Y.L. Optimal configuration of a gas expansion process in a piston-type cylinder with generalized convective heat transfer law. *Energies* **2020**, *13*, 3229. [[CrossRef](#)]
34. Scheunert, M.; Masser, R.; Khodja, A.; Paul, R.; Schwalbe, K.; Fischer, A.; Hoffmann, K.H. Power-optimized sinusoidal piston motion and its performance gain for an Alpha-type Stirling engine with limited regeneration. *Energies* **2020**, *13*, 4564. [[CrossRef](#)]
35. Boikov, S.Y.; Andresen, B.; Akhremenkov, A.A.; Tsirlin, A.M. Evaluation of irreversibility and optimal organization of an integrated multi-stream heat exchange system. *J. Non-Equilib. Thermodyn.* **2020**, *45*, 155–171. [[CrossRef](#)]
36. Chen, L.G.; Feng, H.J.; Ge, Y.L. Maximum energy output chemical pump configuration with an infinite-low- and a finite-high-chemical potential mass reservoirs. *Energy Convers. Manag.* **2020**, *223*, 113261. [[CrossRef](#)]
37. Hoffmann, K.H.; Burzler, J.M.; Schubert, S. Endoreversible thermodynamics. *J. Non-Equilib. Thermodyn.* **1997**, *22*, 311–355.
38. Wagner, K.; Hoffmann, K.H. Endoreversible modeling of a PEM fuel cell. *J. Non-Equilib. Thermodyn.* **2015**, *40*, 283–294. [[CrossRef](#)]
39. Muschik, W. Concepts of phenomenological irreversible quantum thermodynamics I: Closed undecomposed Schottky systems in semi-classical description. *J. Non-Equilib. Thermodyn.* **2019**, *44*, 1–13. [[CrossRef](#)]
40. Ponmurugan, M. Attainability of maximum work and the reversible efficiency of minimally nonlinear irreversible heat engines. *J. Non-Equilib. Thermodyn.* **2019**, *44*, 143–153. [[CrossRef](#)]
41. Raman, R.; Kumar, N. Performance analysis of Diesel cycle under efficient power density condition with variable specific heat of working fluid. *J. Non-Equilib. Thermodyn.* **2019**, *44*, 405–416. [[CrossRef](#)]
42. Schwalbe, K.; Hoffmann, K.H. Stochastic Novikov engine with Fourier heat transport. *J. Non-Equilib. Thermodyn.* **2019**, *44*, 417–424. [[CrossRef](#)]
43. Morisaki, T.; Ikegami, Y. Maximum power of a multistage Rankine cycle in low-grade thermal energy conversion. *Appl. Thermal Eng.* **2014**, *69*, 78–85. [[CrossRef](#)]
44. Yasunaga, T.; Ikegami, Y. Application of finite time thermodynamics for evaluation method of heat engines. *Energy Proc.* **2017**, *129*, 995–1001. [[CrossRef](#)]
45. Yasunaga, T.; Fontaine, K.; Morisaki, T.; Ikegami, Y. Performance evaluation of heat exchangers for application to ocean thermal energy conversion system. *Ocean Thermal Energy Convers.* **2017**, *22*, 65–75.
46. Yasunaga, T.; Koyama, N.; Noguchi, T.; Morisaki, T.; Ikegami, Y. Thermodynamical optimum heat source mean velocity in heat exchangers on OTEC. In Proceedings of the Grand Renewable Energy 2018, Yokohama, Japan, 17–22 June 2018.
47. Yasunaga, T.; Noguchi, T.; Morisaki, T.; Ikegami, Y. Basic heat exchanger performance evaluation method on OTEC. *J. Mar. Sci. Eng.* **2018**, *6*, 32. [[CrossRef](#)]
48. Fontaine, K.; Yasunaga, T.; Ikegami, Y. OTEC maximum net power output using Carnot cycle and application to simplify heat exchanger selection. *Entropy* **2019**, *21*, 1143. [[CrossRef](#)]
49. Yasunaga, T.; Ikegami, Y. Finite-time thermodynamic model for evaluating heat engines in ocean thermal energy conversion. *Entropy* **2020**, *22*, 211. [[CrossRef](#)]
50. Shittu, S.; Li, G.Q.; Zhao, X.D.; Ma, X.L.; Akhlaghi, Y.G.; Fan, Y. Comprehensive study and optimization of concentrated photovoltaic-thermoelectric considering all contact resistances. *Energy Convers. Manag.* **2020**, *205*, 112422. [[CrossRef](#)]
51. Feidt, M. Carnot cycle and heat engine: Fundamentals and applications. *Entropy* **2020**, *22*, 348. [[CrossRef](#)]
52. Feidt, M.; Costea, M. Effect of machine entropy production on the optimal performance of a refrigerator. *Entropy* **2020**, *22*, 913. [[CrossRef](#)] [[PubMed](#)]
53. Ma, Y.H. Effect of finite-size heat source's heat capacity on the efficiency of heat engine. *Entropy* **2020**, *22*, 1002. [[CrossRef](#)] [[PubMed](#)]
54. Rogolino, P.; Cimmelli, V.A. Thermoelectric efficiency of Silicon–Germanium alloys in finite-time thermodynamics. *Entropy* **2020**, *22*, 1116. [[CrossRef](#)] [[PubMed](#)]

55. Dann, R.; Kosloff, R.; Salamon, P. Quantum finite time thermodynamics: Insight from a single qubit engine. *Entropy* **2020**, *22*, 1255. [[CrossRef](#)] [[PubMed](#)]
56. Liu, X.W.; Chen, L.G.; Ge, Y.L.; Feng, H.J.; Wu, F.; Lorenzini, G. Exergy-based ecological optimization of an irreversible quantum Carnot heat pump with spin-1/2 systems. *J. Non-Equilib. Thermodyn.* **2021**, *46*, 61–76. [[CrossRef](#)]
57. Guo, H.; Xu, Y.J.; Zhang, X.J.; Zhu, Y.L.; Chen, H.S. Finite-time thermodynamics modeling and analysis on compressed air energy storage systems with thermal storage. *Renew. Sustain. Energy Rev.* **2021**, *138*, 110656. [[CrossRef](#)]
58. Smith, Z.; Pal, P.S.; Deffner, S. Endoreversible Otto engines at maximal power. *J. Non-Equilib. Thermodyn.* **2020**, *45*, 305–310. [[CrossRef](#)]
59. Chen, L.G.; Shen, J.F.; Ge, Y.L.; Wu, Z.X.; Wang, W.H.; Zhu, F.L.; Feng, H.J. Power and efficiency optimization of open Maisotsenko-Brayton cycle and performance comparison with traditional open regenerated Brayton cycle. *Energy Convers. Manag.* **2020**, *217*, 113001. [[CrossRef](#)]
60. Liu, H.T.; Zhai, R.R.; Patchigolla, K.; Turner, P.; Yang, Y.P. Analysis of integration method in multi-heat-source power generation systems based on finite-time thermodynamics. *Energy Convers. Manag.* **2020**, *220*, 113069. [[CrossRef](#)]
61. Feng, H.J.; Qin, W.X.; Chen, L.G.; Cai, C.G.; Ge, Y.L.; Xia, S.J. Power output, thermal efficiency and exergy-based ecological performance optimizations of an irreversible KCS-34 coupled to variable temperature heat reservoirs. *Energy Convers. Manag.* **2020**, *205*, 112424. [[CrossRef](#)]
62. Feng, J.S.; Gao, G.T.; Dabwan, Y.N.; Pei, G.; Dong, H. Thermal performance evaluation of subcritical organic Rankine cycle for waste heat recovery from sinter annular cooler. *J. Iron. Steel Res. Int.* **2020**, *27*, 248–258. [[CrossRef](#)]
63. Wu, Z.X.; Feng, H.J.; Chen, L.G.; Tang, W.; Shi, J.C.; Ge, Y.L. Constructal thermodynamic optimization for ocean thermal energy conversion system with dual-pressure organic Rankine cycle. *Energy Convers. Manag.* **2020**, *210*, 112727. [[CrossRef](#)]
64. Qiu, S.S.; Ding, Z.M.; Chen, L.G. Performance evaluation and parametric optimum design of irreversible thermionic generators based on van der Waals heterostructures. *Energy Convers. Manag.* **2020**, *225*, 113360. [[CrossRef](#)]
65. Miller, H.J.D.; Mehboudi, M. Geometry of work fluctuations versus efficiency in microscopic thermal machines. *Phys. Rev. Lett.* **2020**, *125*, 260602. [[CrossRef](#)]
66. Gonzalez-Ayala, J.; Roco, J.M.M.; Medina, A.; Calvo Hernández, A. Optimization, stability, and entropy in endoreversible heat engines. *Entropy* **2020**, *22*, 1323. [[CrossRef](#)]
67. Kong, R.; Chen, L.G.; Xia, S.J.; Li, P.L.; Ge, Y.L. Minimizing entropy generation rate in hydrogen iodide decomposition reactor heated by high-temperature helium. *Entropy* **2021**, *23*, 82. [[CrossRef](#)]
68. Albatati, F.; Attar, A. Analytical and experimental study of thermoelectric generator (TEG) system for automotive exhaust waste heat recovery. *Energies* **2021**, *14*, 204. [[CrossRef](#)]
69. Feng, H.J.; Wu, Z.X.; Chen, L.G.; Ge, Y.L. Constructal thermodynamic optimization for dual-pressure organic Rankine cycle in waste heat utilization system. *Energy Convers. Manag.* **2021**, *227*, 113585. [[CrossRef](#)]
70. Garnejani, H.A.; Hossainpou, S.H. Single and multi-objective optimization of a TEG system for optimum power, cost and second law efficiency using genetic algorithm. *Energy Convers. Manag.* **2021**, *228*, 113658. [[CrossRef](#)]
71. Ge, Y.L.; Chen, L.G.; Feng, H.J. Ecological optimization of an irreversible Diesel cycle. *Eur. Phys. J. Plus* **2021**, *136*, 198. [[CrossRef](#)]
72. Chen, L.G.; Meng, F.K.; Ge, Y.L.; Feng, H.J.; Xia, S.J. Performance optimization of a class of combined thermoelectric heating devices. *Sci. China Technol. Sci.* **2020**, *63*, 2640–2648. [[CrossRef](#)]
73. Sahin, B.; Kodal, A.; Yavuz, H. Efficiency of a Joule-Brayton engine at maximum power density. *J. Phys. D Appl. Phys.* **1995**, *28*, 1309–1313. [[CrossRef](#)]
74. Sahin, B.; Kodal, A.; Yavuz, H. Maximum power density analysis of an endoreversible Carnot heat engine. *Energy* **1996**, *21*, 1219–1225. [[CrossRef](#)]
75. Chen, L.G.; Zheng, J.L.; Sun, F.R.; Wu, C. Optimum distribution of heat exchanger inventory for power density optimization of an endoreversible closed Brayton cycle. *J. Phys. D Appl. Phys.* **2001**, *34*, 422–427. [[CrossRef](#)]
76. Chen, L.G.; Zheng, J.L.; Sun, F.R.; Wu, C. Power density optimization for an irreversible closed Brayton cycle. *Open Syst. Inf. Dyn.* **2001**, *8*, 241–260. [[CrossRef](#)]
77. Chen, L.G.; Zheng, J.L.; Sun, F.R.; Wu, C. Performance comparison of an endoreversible closed variable-temperature heat reservoir Brayton cycle under maximum power density and maximum power conditions. *Energy Convers. Manag.* **2002**, *43*, 33–43. [[CrossRef](#)]
78. Chen, L.G.; Zheng, J.L.; Sun, F.R.; Wu, C. Performance comparison of an irreversible closed variable-temperature heat reservoir Brayton cycle under maximum power density and maximum power conditions. *Proc. Inst. Mech. Eng. Part. A J. Power Energy* **2005**, *219*, 559–566. [[CrossRef](#)]
79. Gonca, G. Thermodynamic analysis and performance maps for the irreversible Dual-Atkinson cycle engine (DACE) with considerations of temperature-dependent specific heats, heat transfer and friction losses. *Energy Convers. Manag.* **2016**, *111*, 205–216. [[CrossRef](#)]
80. Gonca, G.; Bahri Sahin, B.; Cakir, M. Performance assessment of a modified power generating cycle based on effective ecological power density and performance coefficient. *Int. J. Exergy* **2020**, *33*, 153–164. [[CrossRef](#)]
81. Karakurt, A.S.; Bashan, V.; Ust, Y. Comparative maximum power density analysis of a supercritical CO₂ Brayton power cycle. *J. Therm. Eng.* **2020**, *6*, 50–57. [[CrossRef](#)]
82. Angulo-Brown, F. An ecological optimization criterion for finite-time heat engines. *J. Appl. Phys.* **1991**, *69*, 7465–7469. [[CrossRef](#)]

83. Yan, Z.J. Comment on “ecological optimization criterion for finite-time heat engines”. *Eur. J. Appl. Physiol.* **1993**, *73*, 3583.
84. Cheng, C.Y.; Chen, C.K. Ecological optimization of an endoreversible Brayton cycle. *Energy Convers. Manag.* **1998**, *39*, 33–44. [[CrossRef](#)]
85. Ma, Z.S.; Chen, Y.; Wu, J.H. Ecological optimization for a combined diesel-organic Rankine cycle. *AIP Adv.* **2019**, *9*, 015320. [[CrossRef](#)]
86. Ahmadi, M.H.; Pourkiaei, S.M.; Ghazvini, M.; Pourfayaz, F. Thermodynamic assessment and optimization of performance of irreversible Atkinson cycle. *Iran. J. Chem. Chem. Eng.* **2020**, *39*, 267–280.
87. Levario-Medina, S.; Valencia-Ortega, G.; Barranco-Jimenez, M.A. Energetic optimization considering a generalization of the ecological criterion in traditional simple-cycle and combined cycle power plants. *J. Non-Equilib. Thermodyn.* **2020**, *45*, 269–290. [[CrossRef](#)]
88. Wu, H.; Ge, Y.L.; Chen, L.G.; Feng, H.J. Power, efficiency, ecological function and ecological coefficient of performance optimizations of an irreversible Diesel cycle based on finite piston speed. *Energy* **2021**, *216*, 119235. [[CrossRef](#)]
89. Kaushik, S.C.; Tyagi, S.K.; Singhal, M.K. Parametric study of an irreversible regenerative Brayton cycle with isothermal heat addition. *Energy Convers. Manag.* **2003**, *44*, 2013–2025. [[CrossRef](#)]
90. Tyagi, S.K.; Kaushik, S.C.; Tiwari, V. Ecological optimization and parametric study of an irreversible regenerative modified Brayton cycle with isothermal heat addition. *Entropy* **2003**, *5*, 377–390. [[CrossRef](#)]
91. Tyagi, S.K.; Chen, J. Performance evaluation of an irreversible regenerative modified Brayton heat engine based on the thermoeconomic criterion. *Int. J. Power Energy Syst.* **2006**, *26*, 66–74. [[CrossRef](#)]
92. Kumar, R.; Kaushik, S.C.; Kumar, R. Power optimization of an irreversible regenerative Brayton cycle with isothermal heat addition. *J. Therm. Eng.* **2015**, *1*, 279–286. [[CrossRef](#)]
93. Tyagi, S.K.; Chen, J.; Kaushik, S.C. Optimum criteria based on the ecological function of an irreversible intercooled regenerative modified Brayton cycle. *Int. J. Exergy* **2005**, *2*, 90–107. [[CrossRef](#)]
94. Tyagi, S.K.; Wang, S.; Kaushik, S.C. Irreversible modified complex Brayton cycle under maximum economic condition. *Indian J. Pure Appl. Phys.* **2006**, *44*, 592–601.
95. Tyagi, S.K.; Chen, J.; Kaushik, S.C.; Wu, C. Effects of intercooling on the performance of an irreversible regenerative modified Brayton cycle. *Int. J. Power Energy Syst.* **2007**, *27*, 256–264. [[CrossRef](#)]
96. Tyagi, S.K.; Wang, S.; Park, S.R. Performance criteria on different pressure ratios of an irreversible modified complex Brayton cycle. *Indian J. Pure Appl. Phys.* **2008**, *46*, 565–574.
97. Wang, J.H.; Chen, L.G.; Ge, Y.L.; Sun, F.R. Power and power density analyzes of an endoreversible modified variable-temperature reservoir Brayton cycle with isothermal heat addition. *Int. J. Low-Carbon Technol.* **2016**, *11*, 42–53. [[CrossRef](#)]
98. Wang, J.H.; Chen, L.G.; Ge, Y.L.; Sun, F.R. Ecological performance analysis of an endoreversible modified Brayton cycle. *Int. J. Sustain. Energy* **2014**, *33*, 619–634. [[CrossRef](#)]
99. Tang, C.Q.; Feng, H.J.; Chen, L.G.; Wang, W.H. Power density analysis and multi-objective optimization for a modified endoreversible simple closed Brayton cycle with one isothermal heating process. *Energy Rep.* **2020**, *6*, 1648–1657. [[CrossRef](#)]
100. Arora, R.; Kaushik, S.C.; Kumar, R.; Arora, R. Soft computing based multi-objective optimization of Brayton cycle power plant with isothermal heat addition using evolutionary algorithm and decision making. *Appl. Soft Comput.* **2016**, *46*, 267–283. [[CrossRef](#)]
101. Arora, R.; Arora, R. Thermodynamic optimization of an irreversible regenerated Brayton heat engine using modified ecological criteria. *J. Therm. Eng.* **2020**, *6*, 28–42. [[CrossRef](#)]
102. Chen, L.G.; Tang, C.Q.; Feng, H.J.; Ge, Y.L. Power, efficiency, power density and ecological function optimizations for an irreversible modified closed variable-temperature reservoir regenerative Brayton cycle with one isothermal heating process. *Energies* **2020**, *13*, 5133. [[CrossRef](#)]
103. Qi, W.; Wang, W.H.; Chen, L.G. Power and efficiency performance analyses for a closed endoreversible binary Brayton cycle with two isothermal processes. *Therm. Sci. Eng. Prog.* **2018**, *7*, 131–137. [[CrossRef](#)]
104. Tang, C.Q.; Chen, L.G.; Feng, H.J.; Wang, W.H.; Ge, Y.L. Power optimization of a closed binary Brayton cycle with isothermal heating processes and coupled to variable-temperature reservoirs. *Energies* **2020**, *13*, 3212. [[CrossRef](#)]
105. Ahmadi, M.H.; Dehghani, S.; Mohammadi, A.H.; Feidt, M.; Barranco-Jimenez, M.A. Optimal design of a solar driven heat engine based on thermal and thermo-economic criteria. *Energy Convers. Manag.* **2013**, *75*, 635–642. [[CrossRef](#)]
106. Ahmadi, M.H.; Mohammadi, A.H.; Dehghani, S.; Barranco-Jimenez, M.A. Multi-objective thermodynamic-based optimization of output power of Solar Dish-Stirling engine by implementing an evolutionary algorithm. *Energy Convers. Manag.* **2013**, *75*, 438–445. [[CrossRef](#)]
107. Ahmadi, M.H.; Ahmadi, M.A.; Mohammadi, A.H.; Feidt, M.; Pourkiaei, S.M. Multi-objective optimization of an irreversible Stirling cryogenic refrigerator cycle. *Energy Convers. Manag.* **2014**, *82*, 351–360. [[CrossRef](#)]
108. Ahmadi, M.H.; Ahmadi, M.A.; Mehrpooya, M.; Hosseinzade, H.; Feidt, M. Thermodynamic and thermo-economic analysis and optimization of performance of irreversible four-temperature-level absorption refrigeration. *Energy Convers. Manag.* **2014**, *88*, 1051–1059. [[CrossRef](#)]
109. Ahmadi, M.H.; Ahmadi, M.A. Thermodynamic analysis and optimization of an irreversible Ericsson cryogenic refrigerator cycle. *Energy Convers. Manag.* **2015**, *89*, 147–155. [[CrossRef](#)]

110. Jokar, M.A.; Ahmadi, M.H.; Sharifpur, M.; Meyer, J.P.; Pourfayaz, F.; Ming, T.Z. Thermodynamic evaluation and multi-objective optimization of molten carbonate fuel cell-supercritical CO₂ Brayton cycle hybrid system. *Energy Convers. Manag.* **2017**, *153*, 538–556. [[CrossRef](#)]
111. Han, Z.H.; Mei, Z.K.; Li, P. Multi-objective optimization and sensitivity analysis of an organic Rankine cycle coupled with a one-dimensional radial-inflow turbine efficiency prediction model. *Energy Convers. Manag.* **2018**, *166*, 37–47. [[CrossRef](#)]
112. Ghasemkhani, A.; Farahat, S.; Naserian, M.M. Multi-objective optimization and decision making of endoreversible combined cycles with consideration of different heat exchangers by finite time thermodynamics. *Energy Convers. Manag.* **2018**, *171*, 1052–1062. [[CrossRef](#)]
113. Ahmadi, M.H.; Jokar, M.A.; Ming, T.Z.; Feidt, M.; Pourfayaz, F.; Astaraei, F.R. Multi-objective performance optimization of irreversible molten carbonate fuel cell–Braysson heat engine and thermodynamic analysis with ecological objective approach. *Energy* **2018**, *144*, 707–722. [[CrossRef](#)]
114. Wang, M.; Jing, R.; Zhang, H.R.; Meng, C.; Li, N.; Zhao, Y.R. An innovative Organic Rankine Cycle (ORC) based Ocean Thermal Energy Conversion (OTEC) system with performance simulation and multi-objective optimization. *Appl. Therm. Eng.* **2018**, *145*, 743–754. [[CrossRef](#)]
115. Patela, V.K.; Raja, B.D. A comparative performance evaluation of the reversed Brayton cycle operated heat pump based on thermo-ecological criteria through many and multi-objective approaches. *Energy Convers. Manag.* **2019**, *183*, 252–265. [[CrossRef](#)]
116. Hu, S.Z.; Li, J.; Yang, F.B.; Yang, Z.; Duan, Y.Y. Multi-objective optimization of organic Rankine cycle using hydrofluorolefins (HFOs) based on different target preferences. *Energy* **2020**, *203*, 117848. [[CrossRef](#)]
117. Hu, S.Z.; Li, J.; Yang, F.B.; Yang, Z.; Duan, Y.Y. How to design organic Rankine cycle system under fluctuating ambient temperature: A multi-objective approach. *Energy Convers. Manag.* **2020**, *224*, 113331. [[CrossRef](#)]
118. Sun, M.; Xia, S.J.; Chen, L.G.; Wang, C.; Tang, C.Q. Minimum entropy generation rate and maximum yield optimization of sulfuric acid decomposition process using NSGA-II. *Entropy* **2020**, *22*, 1065. [[CrossRef](#)] [[PubMed](#)]
119. Sadeghi, S.; Ghandehariun, S.; Naterer, G.F. Exergoeconomic and multi-objective optimization of a solar thermochemical hydrogen production plant with heat recovery. *Energy Convers. Manag.* **2020**, *225*, 113441. [[CrossRef](#)]
120. Wu, Z.X.; Feng, H.J.; Chen, L.G.; Ge, Y.L. Performance optimization of a condenser in ocean thermal energy conversion (OTEC) system based on constructal theory and multi-objective genetic algorithm. *Entropy* **2020**, *22*, 641. [[CrossRef](#)]
121. Ghorani, M.M.; Haghighi, M.H.S.; Riasi, A. Entropy generation minimization of a pump running in reverse mode based on surrogate models and NSGA-II. *Int. Commun. Heat Mass Transfer* **2020**, *118*, 104898. [[CrossRef](#)]
122. Wang, L.B.; Bu, X.B.; Li, H.S. Multi-objective optimization and off-design evaluation of organic Rankine cycle (ORC) for low-grade waste heat recovery. *Energy* **2020**, *203*, 117809. [[CrossRef](#)]
123. Herrera-Orozco, I.; Valencia-Ochoa, G.; Jorge Duarte-Forero, J. Exergo-environmental assessment and multi-objective optimization of waste heat recovery systems based on Organic Rankine cycle configurations. *J. Clean. Prod.* **2021**, *288*, 125679. [[CrossRef](#)]
124. Shi, S.S.; Ge, Y.L.; Chen, L.G.; Feng, F.J. Four objective optimization of irreversible Atkinson cycle based on NSGA-II. *Entropy* **2020**, *22*, 1150. [[CrossRef](#)]
125. Tang, W.; Feng, H.J.; Chen, L.G.; Xie, Z.J.; Shi, J.C. Constructal design for a boiler economizer. *Energy* **2021**, *223*, 120013. [[CrossRef](#)]
126. Chen, L.G.; Zheng, J.L.; Sun, F.R.; Wu, C. Power density optimization for an irreversible regenerated closed Brayton cycle. *Phys. Scripta* **2001**, *64*, 184–191. [[CrossRef](#)]
127. Bejan, A. *Entropy Generation through Heat and Fluid Flow*; Wiley: New York, NY, USA, 1982.
128. Bejan, A. Theory of heat transfer-irreversible power plant. *Int. J. Heat Mass Transfer* **1988**, *31*, 1211–1219. [[CrossRef](#)]
129. Bejan, A. The equivalence of maximum power and minimum entropy generation rate in the optimization of power plants. *J. Energy Res. Tech.* **1996**, *118*, 98–101. [[CrossRef](#)]
130. Bejan, A. Models of power plants that generate minimum entropy while operating at maximum power. *Am. J. Phys.* **1996**, *64*, 1054–1059. [[CrossRef](#)]
131. Salamon, P.; Hoffmann, K.H.; Schubert, S.; Berry, R.S.; Andresen, B. What conditions make minimum entropy production equivalent to maximum power production? *J. Non-Equilib. Thermodyn.* **2001**, *26*, 73–83. [[CrossRef](#)]
132. Andresen, B.; Berry, R.S.; Nitzan, A.; Salamon, P. Thermodynamics in finite time: The step-Carnot cycle. *Phys. Rev. A* **1977**, *15*, 2086–2093. [[CrossRef](#)]
133. Orlov, V.N.; Rudenko, A.V. Optimal control in problems of extremal of irreversible thermodynamic processes. *Avtomatika Telemekhanika* **1985**, *46*, 549–577.
134. Lu, P.C. Thermodynamics with finite heat-transfer area or finite surface thermodynamics. *Thermodynamics and the Design, Analysis, and Improvement of Energy Systems*, ASME Adv. Energy Sys. Div. Pub. AES **1995**, *35*, 51–60.
135. Bejan, A. Entropy generation minimization: The new thermodynamics of finite size devices and finite time processes. *J. Appl. Phys.* **1996**, *79*, 1191–1218. [[CrossRef](#)]
136. Feidt, M. *Thermodynamique et Optimisation Energetique des Systems et Procèdes*, 2nd ed.; Technique et Documentation, Lavoisier: Paris, France, 1996. (In French)
137. Dong, Y.; El-Bakkali, A.; Feidt, M.; Descombes, G.; Perilhon, C. Association of finite-dimension thermodynamics and a bond-graph approach for modeling an irreversible heat engine. *Entropy* **2012**, *14*, 1234–1258. [[CrossRef](#)]
138. Feidt, M. *Thermodynamique Optimale en Dimensions Physiques Finies*; Hermès: Paris, France, 2013.

139. Perescu, S.; Costea, M.; Feidt, M.; Ganea, I.; Boriaru, N. *Advanced Thermodynamics of Irreversible Processes with Finite Speed and Finite Dimensions*; Editura AGIR: Bucharest, Romania, 2015.
140. Feidt, M. *Finite Physical Dimensions Optimal Thermodynamics 1. Fundamental*; ISTE Press and Elsevier: London, UK, 2017.
141. Feidt, M. *Finite Physical Dimensions Optimal Thermodynamics 2. Complex. Systems*; ISTE Press and Elsevier: London, UK, 2018.
142. Blaise, M.; Feidt, M.; Maillet, D. Influence of the working fluid properties on optimized power of an irreversible finite dimensions Carnot engine. *Energy Convers. Manag.* **2018**, *163*, 444–456. [[CrossRef](#)]
143. Feidt, M.; Costea, M. From finite time to finite physical dimensions thermodynamics: The Carnot engine and Onsager's relations revisited. *J. Non-Equilib. Thermodyn.* **2018**, *43*, 151–162. [[CrossRef](#)]
144. Dumitrascu, G.; Feidt, M.; Popescu, A.; Grigorean, S. Endoreversible trigeneration cycle design based on finite physical dimensions thermodynamics. *Energies* **2019**, *12*, 3165. [[CrossRef](#)]
145. Feidt, M.; Costea, M. Progress in Carnot and Chambadal modeling of thermomechanical engine by considering entropy and heat transfer entropy. *Entropy* **2019**, *21*, 1232. [[CrossRef](#)]
146. Feidt, M.; Costea, M.; Feidt, R.; Danel, Q.; Périlhon, C. New criteria to characterize the waste heat recovery. *Energies* **2020**, *13*, 789. [[CrossRef](#)]